DE- SC0006410, Jonathan S. Owen,
Department of Chemistry, Columbia University
Project period: 07/2011-2016

Measuring the Importance of Valence to the Chemistry of Nanocrystal Surfaces

November 30, 2016

ABSTRACT

The goal of this project is to understand and control the interplay between nanocrystal stoichiometry, surface ligand binding and exchange, and the optoelectronic properties of semiconductor nanocrystals in solution and in thin solid films. We pursued three research directions with this goal in mind: 1) We characterized nanocrystal stoichiometry and its influence on the binding of L-type and X-type ligands, including the thermodynamics of binding and the kinetics of ligand exchange. 2) We developed a quantitative understanding of the relationship between surface ligand passivation and photoluminescence quantum yield. 3) We developed methods to replace the organic ligands on the nanocrystal with halide ligands and controllably deposit these nanocrystals into thin films, where electrical measurements were used to investigate the electrical transport and internanocrystal electronic coupling.

RESEARCH ACCOMPLISHMENTS

The Coordination Chemistry of II-VI Nanocrystals. The frontier orbitals of inorganic semiconductors are typically derived from defects. The electronic states created by impurities and surfaces, for example, tend to fall within the band gap and can trap electrical charges and cause exciton recombination. Roughly half the atoms in nanometer scale crystals are found at surfaces and therefore surface derived orbitals tend to dominate their optoelectronic properties. As a result, the photoluminescence quantum yield and electron transfer characteristics of nanocrystals depend sensitively on surface structure. Broadly speaking, gaining control over surfaces is one of the most important challenges of semiconductor science and an atomic scale understanding of surface structure and reactivity is sorely needed to do so. We aim to create this understanding by developing a coordination chemistry of nanocrystal surfaces.

Scheme 1. Nanocrystal ligand binding motifs as classified by the L,X,Z, formalism.

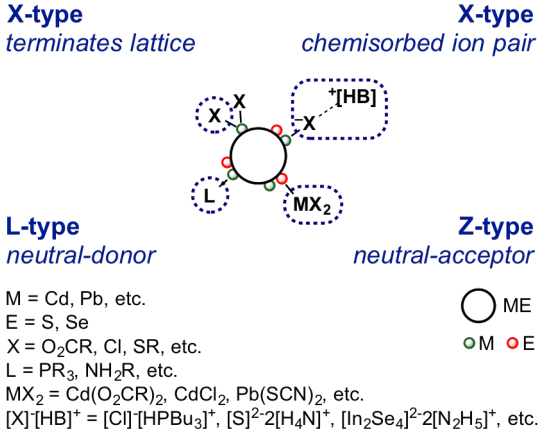

My lab's work has shown that the binding of ligands to nanocrystals is heavily influenced by

the metal chalcogenide stoichiometry. For example, metal chalcogenide nanocrystals are typically rich in cations that adsorb to the crystals surface. These cations balance charge with ligand anions, otherwise known as X-type ligands within the covalent bond classification method developed by M.L.H. Green (Scheme 1).i,ii On the other hand a stoichiometric metal chalcogenide nanocrystal is charge neutral and binds neutral L-type ligands and adsorbs ion pairs to its Lewis acidic metal sites. Distinguishing between ligation types in this way seeks to describe the nanocrystal as a molecular complex, and to illustrate the importance of charge balance to nanocrystal chemical formulas. Although intuitive to chemists, this approach is novel within materials science and is gaining acceptance as the preferred way to describe nanocrystal-ligand interactions. Indeed, our introduction of Green's covalent bond classification scheme to describe nanocrystal ligation is gaining broad traction within the field and improving contemporary descriptions of nanocrystal reactivity. Below are several examples where we have explored the relationship between nanocrystal formula, ligand exchange reactivity, and optoelectronic properties using this description as a guide.

Chloride-Terminated Nanocrystals. Removing organic surfactant ligands from nanocrystal surfaces is required to transform these soluble materials into thin-films that efficiently transport electrical charge. We have developed a technique to cleave carboxylate and phosphonate ligands in exchange for a layer of halide ligands by reaction with halotrimethylsilanes (Scheme 2).[iii] In the presence of trialkylphosphine supporting ligands, soluble chloride terminated nanocrystals can be isolated and characterized using ^{1}H and ^{31}P NMR spectroscopy. The wide chemical shift range

Scheme 2. Carboxylate for chloride exchange in the presence tri-*n*-butylphosphine (Bu_3P).[a]

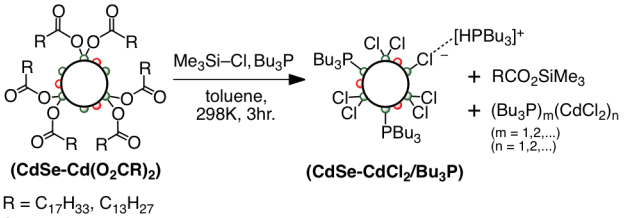

[a] Red circles = Se, green circles = Cd, large white circle = a stoichiometric cadmium selenide crystal.

Scheme 3. Chloride terminated nanocrystal thin films from soluble inks.[a]

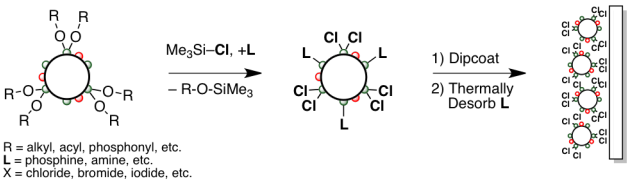

Figure 1. Thermal annealing of nanocrystal thin films *en vacuo* as monitored by FT-IR (A), UV-Vis (B), grazing incidence x-ray diffraction and electrical transport (C,D).[a]

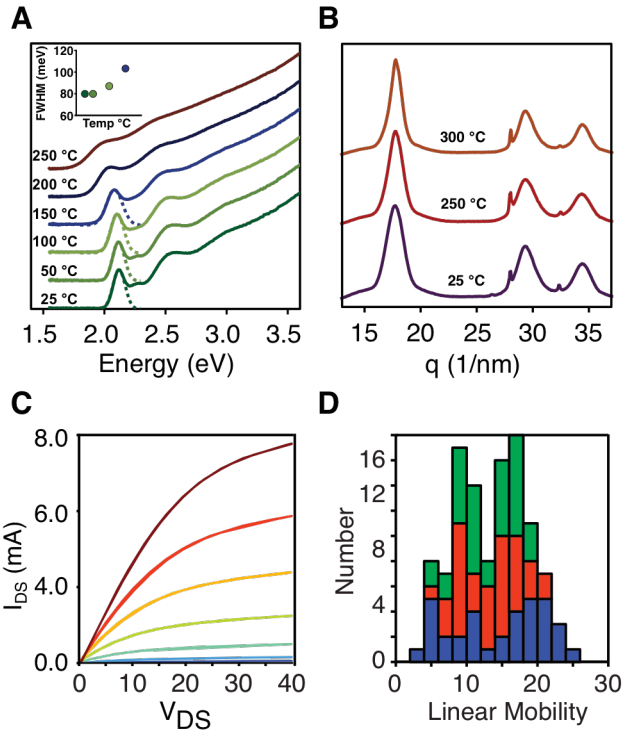

of ^{31}P NMR spectra allowed us to identify the diversity of ligand types, and ultimately led to the L,X,Z classification shown in Scheme 1. Detailed measurements of ligand coverages indicate that purified cadmium selenide nanocrystals contain 2.5 – 3.5 carboxylate ligands nm^{-2} of surface area prior to cleavage. These are replaced by chloride anions as well as tri-*n*-alkylphosphine coligands that display a low surface coverage at saturation (0.5 nm^{-2}).

Thin Solid Films of Halide Terminated Nanocrystals. Methods to fabricate semiconductor devices using solution techniques are desired for flexible electronics and low cost, high throughput manufacturing. Our halide exchange methods are ideal for this purpose because the organic supporting ligands can be desorbed under vacuum. Thus, solutions of chloride terminated nanocrystals can be used as an ink to cast thin semiconductor films (Scheme 3).[iv] The electrical conductivity in these films is dramatically enhanced upon desorption of the datively bound organic ligand shell. In principle, close internanocrystal contacts will lead to delocalized electrical carriers and high charge transport mobilities, a goal being pursued by many groups. Using a combination of UV-visible absorption (Figure 1A), grazing incidence x-ray scattering (Figure 1B), and electron microscopy we have monitored the desorption of the organic ligand shell and the delocalization of excitonic states within the film as the film sinters and the nanocrystalline grains fuse. Thin film transistors fabricated using this approach display n-type conductivity (Figure 2C and 2D) and electron mobilities as high as 25 cm^2 V^{-1} sec^{-1}, a world-record for solution processed thin films of cadmium selenide nanocrystals and similar to vacuum deposited thin films. X-ray scattering as a function of the annealing condition supports a sintering scheme where isolated nanocrystals undergo a fusion reaction that

Scheme 4. Three stages of nanocrystal sintering during thermal annealing.

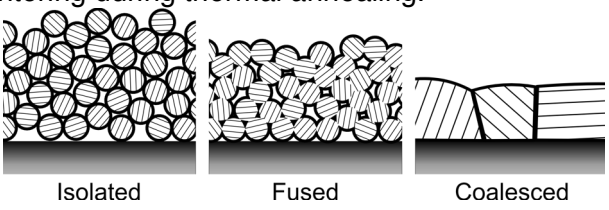

Scheme 5. Displacement of L-M(O_2CR)$_2$ from metal chalcogenide nanocrystals promoted by L-type ligands.

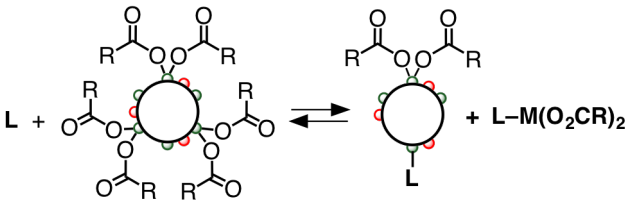

M = Cd, Pb
E = S, Se
R = alkyl, oleyl
L = Bu_3P, $BuNH_2$, C_5H_5N, TMEDA, etc.

ME
M E

Figure 2. Photoluminescence quantum yield versus the coverage of cadmium carboxylate..[a]

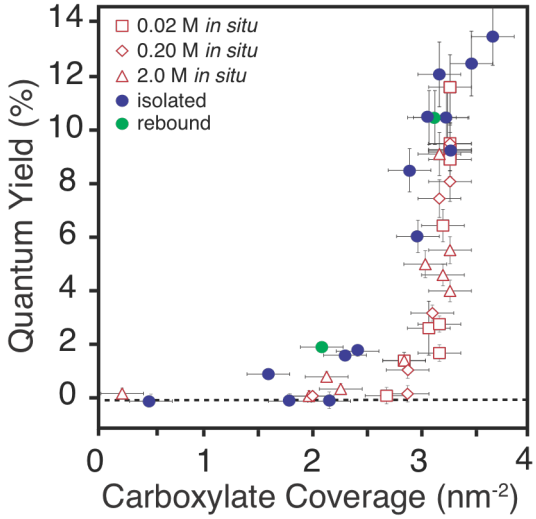

[a] Empty red shapes taken from *in situ* measurements with displacement reagents present. Filled circles correspond to samples where the coverage was measured after isolation following displacement (blue) or rebinding (green) of Cd(O_2CR)$_2$.

dramatically enhances the intergrain contact and the electron transport mobilities (Scheme 4). Our work clearly demonstrates that this strucutural transition is necessary to achieve high mobilitieis. However, it also demonstrated that thin films with nanocrystalline grain size can achieve high charge transport mobilities.

Nanocrystal Stoichiometry and Photoluminescence Quantum Yield. Since 2008, nanocrystal stoichiometry has been investigated for of its relevance to surface coordination chemistry.[v] Prior to that time, it was implicitly assumed that ligands were exclusively L-type donors that reversibly absorb to the nanocrystals surface, tri-*n*-octylphosphine oxide being a canonical example. It has remained a mystery how observations of reversible ligand binding can be reconciled with the picture shown in Scheme 1, where X-type ligands balance charge with the excess cations of a metal rich nanocrystal. We have discovered that the cadmium and lead cations along with their carboxylate anions are very labile and can be rapidly and reversibly displaced from nanocrystal surfaces by Lewis bases (Scheme 4).[vi] In other words, cadmium and lead chalcogenide nanocrystals have dynamic chemical formulas and are in rapid equilibrium with metal carboxylate complexes freely diffusing in solution.

The displacement potency of a variety of neutral donor ligands was surveryed and found to depend sensitively on steric factors (Scheme 5). These results suggest that the displacement equilibrium is driven by ligand binding to the nanocrystal as well as the soluble metal carboxylate complexes. Solvents used to manipulate and purify nanocrystals also displace cadmium carboxylate, though to a lesser extent. Moreover, the reactivity of cadmium sulfide, lead sulfide, and lead selenide nanocrystals is similar, making this a general mode of reactivity for the most widely studied classes of semiconductor nanocrystals. Recently we have used this approach to prepare the first examples of purely stoichiometric nanocrystals stabilized exclusively by L-type ligands. These nanocrystals provide a valuable synthon with which to study metal carboxylate binding reactivity and with which to make cadmium selenide thin films without ligands, a highly sought after sample.

Scheme 6. Orbital interaction diagram illustrating the "passivation" of surface selenium states by adsorption of cadmium carboxylate.[a]

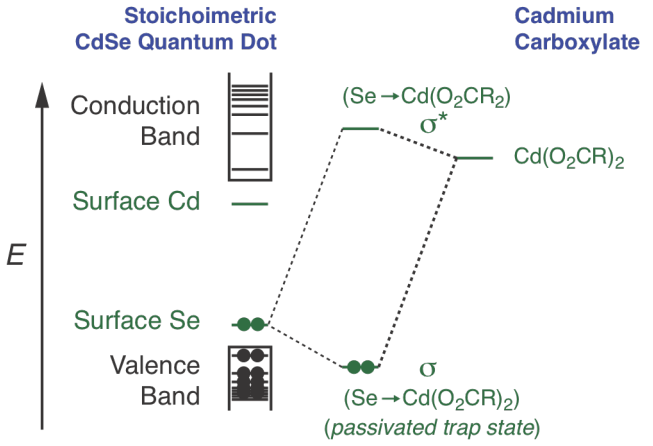

Figure 3. Time resolved photoluminescence demonstrating fast hole trapping that is sensitive to carboxylate coverage.[a]

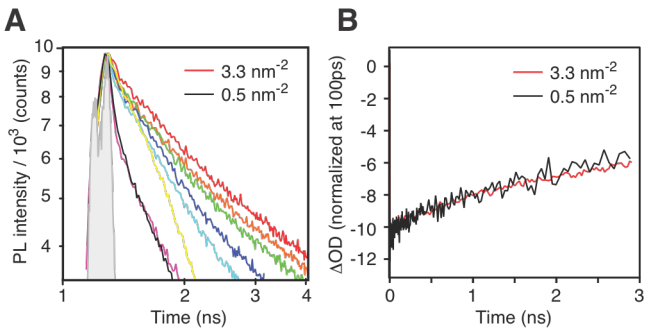

[a] Decreasing carboxylate coverage (3.3 nm^{-2} to 0.5 nm^{-2}) and causes a steady increase in the rate of hole trapping as evidenced by the decreased PL lifetime and the steady transient absorption bleach recovery.

Nanocrystal Stoichiometry and Surface State Passivation. The lability of surface metal ions has significant consequences for nanocrystal electronic structure and photoluminescence quantum yield. In Figure 2 the photoluminescence quantum yield of cadmium selenide nanocrystals is plotted versus their coverage of carboxylate ligands. This is the first quantitative data relating the coverage of any ligand type and photoluminescence quantum yield and clarifies several important relationships and raises many interesting questions. Foremost, the photoluminescence quantum yield is found to depend very sensitively to coverage near saturation. Combined with the facile displacement reactivity described above it is clear that slight modifications of the solution conditions might only slightly change the formula but will dramatically influence exciton recombination. This conclusion helps explain the large number of conflicting and irreproducible studies of photoluminescence quantum yield. It also clearly demonstrates the importance of careful synthetic and analytical chemistry; nanocrystal scientists must gain precise control over stoichiometry in order to draw general conclusions regarding nanocrystal optoelectronic properties.

In collaboration with Matt Sfeir at Lawrence Berkeley National Laboratory we have investigated the charge trapping dynamics in cadmium selenide nanocrystals as a function of cadmium carboxylate coverage (Scheme 6 and Figure 3). By comparing time resolved photoluminescence and transient absorption data, we demonstrate that as the cadmium coverage is lowered the rate of hole trapping increases. A comprehensive kinetic model that accounts for the fraction of "dark" nanocrystals explains the dependence of the photoluminescence quantum yeild on the carboxylate coverage shown in Figure 5. Mechanistic insights that directly link surface structure, electronic structure, and exciton recombination are uncommon and are good evidence that our structural studies are having the broad impact on nanocrystal research that we intended.

Tight Binding of Anionic Ligands to Stoichiometric Nanocrystals. Using the displacement reactivity described above we have isolated stoichiometric CdSe nanocrystals stabilized by *n*-alkylamine ligands. To achieve this goal we first developed a method to remove oleic acid impurities that are present in the nanocrystal starting material, and lead to the formation of adsorbed ammonium oleate. By first removing the carboxylic acid impurities, we could isolate nanocrystals solely stabilized by amine ligands. With amine bound nanocrystals in hand, we demonstrated that phosphonate and carbamate ions can form from a reaction between the amine ligands and carboxylic or phosphonic acids and carbon dioxide, respectively. In each case, the anion binds the surface with much greater affinity than the neutral amine ligand and remains tightly associated, even in concentrated amine solution. These ion pairs are difficult to detect and can be easily confused with

Scheme 7. Ion pair stabilization by nanocrystal surface.

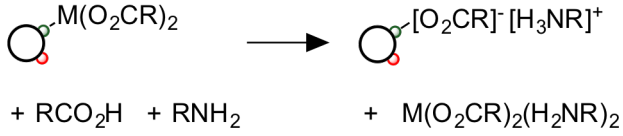

Scheme 8. Addition of acidic molecules to amine bound CdSe leads to the formation of adsorbed ion pairs.

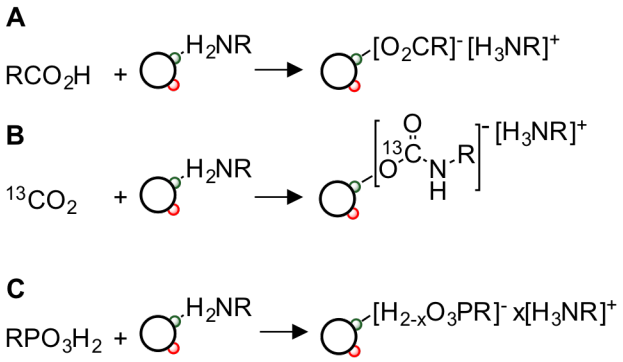

neutral amine ligands and cadmium phosphonate ligands. These observations strongly suggest that such ion pairs are much more pervasive than previously thought, and help explain the challenge of completely removing ligands from nanocrystal surfaces.

Summary We have discovered that surface bound metal ions are labile and rapidly equilibrate with the solution. Careful measurements of nanocrystal stoichiometry have shown that photoluminescence quantum yields depend sensitively on the coverage of cadmium carboxylate. Binding of cadmium carboxylate passivates surface selenium atoms and guards against hole trapping. In addition, we have investigated the competitive binding of L-type ligands and determined factors that control the relative affinity for the nanocrystals surface. Somewhat to our surprise, steric factors sensitively influence the binding affinities, with the least sterically encumbered ligands having the greatest affinities and reaching the highest coverages. Moreover, we demonstrated that neutral amine ligands react with acidic molecules to form tightly bound ion pairs that are difficult to distinguish from neutral amines and anionic ligands that balance charge with a metal-enriched nanocrystal.

E. ARTICLES RESULTING FROM THIS GRANT

Submitted

(1) "Tight Binding of Carboxylate, Phosphonate, and Carbamate Anions to Stoichiometric CdSe Nanocrystals" Chen, P.E.; Norman, Z.M.; Anderson, N.C.; Owen, J.S.; *Submitted*.

(2) "A Tunable Library of Selenourea Precursors to PbSe Nanocrystals with Size Distributions Near that Homogeneous Limit" Campos, M.; Hendricks, M.P.; Beecher, A.N.; Swain, R.A.; Cleveland, G. T.; Sfeir, M.Y.; Owen, J.S.; *Submitted*.

Published

(3) "Synthesis, Structures and Reactivity of [Tm^{tBu}]ZnH, a Monomeric Terminal Zinc Hydride Compound in a Sulfur-Rich Coordination Environment: Access to a Heterobimetallic Compound" Krieder-Mueller, A.; Quinlivan, P.; Rauch, M.; Owen, J.S.; Parkin, G.; *Chem. Comm.* **2016**, *52*, 2358–2361.

(4) "Synthesis and Surface Chemistry of Cadmium Carboxylate Passivated CdTe Nanocrystals from Cadmium *bis*(phenyltellurolate)" Campos, M.P.; Owen, J.S.; *Chem. Mater.* **2016**, *28(1)*, 227-233.

(5) "The Effect of Surface Stoichiometry on Blinking and Hole Trapping Dynamics in CdSe Nanocrystals" Anderson, Busby, E.; N.C.; Owen, J.S.; Sfeir, M.E *J. Phys. Chem. C* **2015**, *119*(49), 27797-27803.

(6) "Exchange of Alkyl and Tris(2-mercapto-1-*t*-butylimidazolyl)hydroborato Ligands Between Zinc, Cadmium and Mercury" Kreider-Mueller, A.; Quinlivan, P.J.; Rong, Y.; Owen, J.S.; Parkin, G.; *J. Organomet. Chem.* **2015**, *792*, 177-183.

(7) "Synthesis and Structures of Cadmium Carboxylate and Thiocarboxylate Compounds with a Sulfur-Rich Coordination Environment: Carboxylate Exchange Kinetics Involving Tris(2-mercapto-1-t-butylimidazolyl)hydroborato Cadmium Complexes, $[Tm^R]Cd(O_2CR)$" Krieder-Mueller, A.; Quinlivan, P.; Rong, Y.; Owen, J.S.; Parkin, G.; *Inorg. Chem.* **2015,** *ASAP*.

(8) "A Tunable Library of Precursors to Metal Sulfide Nanocrystals", Hendricks, M.P.; Campos, M.P.; Cleveland, G.T.; Jen-La Plante, I.; Owen, J.S.; *Science* **2015**, *348*(6240), 1226-1230.

(9) "Synthesis and Structures of Cadmium Carboxylate and Thiocarboxylate Compounds with a Sulfur-Rich Coordination Environment: Carboxylate Exchange Kinetics Involving Tris(2-mercapto-1-t-butylimidazolyl)hydroborato Cadmium Complexes, $[Tm^R]Cd(O_2CR)$" Krieder-Mueller, A.; Quinlivan, P.; Rong, Y.; Owen, J.S.; Parkin, G.; *Inorg. Chem.,* **2015,** *54*(8), 3835-3850.

(10) "The Coordination Chemistry of Nanocrystal Surfaces" Owen, J.S.: *Science,* **2015**, *347*(6222), 615-616**.**

(11) "Electrical Transport and Grain Growth in Chloride-Terminated Cadmium Selenide Nanocrystal Thin Films" Norman, Z.M.; Anderson, N.C.; Owen J.S.; *ACS Nano* **2014***, 8*(7), 7513-7521.

(12) "Ligand Exchange and the Stoichiometry of Metal-Chalcogenide Nanocrystals: Spectroscopic Observation of Facile Metal-Carboxylate Binding and Displacement." Anderson, N. C.; Hendricks, M. P.; Choi. J. J.; Owen, J. S.; *J. Am. Chem. Soc.* **2013**, *135*, 18536-18548.

(13) "Soluble Chloride-Terminated Cadmium Selenide Nanocrystals: Ligand Exchange Monitored by ^{1}H and ^{31}P NMR spectroscopy", Anderson, N. C.; Owen, J. S.; *Chem. Mater.* **2013**, *25*, 69-76.

F. PERSONNEL

Graduate Students
Michael Campos (100% support)
Peter Chen (NSF, Graduate Research Fellow) (0% support)
Zachariah Norman (100% support)
Iva Rreza (25% support)
Ava Krieder-Mueller (50% support)
Nicholas Anderson (NSF, Graduate Research Fellow) (0% support)
Undergraduate Students
Robert Swain (0% support)
Gregory Cleveland (0% support)
Collaborators
Matthew Sfeir (Brookhaven National Laboratory, 0% support)
Eric Busby (Brookhaven National Laboratory, 0% support)
Simon Billinge (Columbia University, 0% support)

G. ESTIMATED UNEXPENDED FUNDS

In each year of the grant we have spent the budget in full.

REFERENCES

[i] "A New Approach to the Formal Classification of Covalent Compounds of the Elements." M.L.H. Green, *J. Organomet. Chem.*, **1995**, *500,* 127-148.

[ii] "The Coordination Chemistry of Nanocrystal Surfaces" **Owen, J.S.**: *Science,* **2015**, *347*(6222), 615-616**.** (*Invited Perspective Article*)

[iii] "Soluble Chloride-Terminated Cadmium Selenide Nanocrystals: Ligand Exchange Monitored by ^{1}H and ^{31}P NMR Spectroscopy" Anderson, N.C.; **Owen, J.S.**; *Chem. Mater.* **2013**, *25*, 69-76.

[iv] "Electrical Transport and Grain Growth in Chloride-Terminated Cadmium Selenide Nanocrystal Thin Films" Norman, Z.M.; Anderson, N.C.; **Owen J.S.;** *ACS Nano.* **2014***, 8*(7), 7513-7521.

[v] "Reaction Chemistry and Ligand Exchange at Cadmium Selenide Nanocrystal Surfaces" Owen, J.S.; Park, J.; Trudeau, P.-E.; Alivisatos, A.P.; *J. Am. Chem. Soc.* **2008**, *130*, 12279-12281.

[vi] "Ligand Exchange and the Stoichiometry of Metal-Chalcogenide Nanocrystals: Spectroscopic Observation of Facile Metal-Carboxylate Binding and Displacement" Anderson, N.C.; Hendricks, M.P.; Choi. J.J.; **Owen, J.S.**; *J. Am. Chem. Soc.* **2013**, *135*, 18536-18548.

Tight Binding of Carboxylate, Phosphonate, and Carbamate Anions to Stoichiometric CdSe Nanocrystals

*Peter E. Chen, Zachariah M. Norman, Nicholas C. Anderson, and Jonathan S. Owen**

Department of Chemistry, Columbia University, 3000 Broadway, MC 3121, New York, NY 10027.
jso2115@columbia.edu

ABSTRACT. The presence of acidic impurities in cadmium selenide nanocrystal systems and their impact on ion-pair formation is presented. Dimethylcadmium (Me_2Cd) and diethylzinc (Et_2Zn) are used to scavenge carboxylic acids from carboxylate-terminated cadmium selenide nanocrystals, CdSe[$Cd(O_2CR)_2$/HO_2CR] leading to the formation of methane, ethane, and metal carboxylate coproducts. Reaction with Me_2Cd also produces surface bound methyl groups (δ = 0.4 ppm, 0.04–0.22 nm^{-2}) that photolytically dissociate to methyl radicals and *n*-doped nanocrystals. Only following the removal of acidic impurities can surface-bound carboxylates be completely displaced using *n*-alkylamine ligands (CdSe[NH_2R], R = *n*-butyl, *n*-hexyl, *n*-octyl) (≤ 0.01 carboxylates/nm^2). Carbon dioxide, oleic acid, and *n*-octadecylphosphonic acid react with CdSe[NH_2R] to form surface-bound *n*-alkylammonium oleate, phosphonate, and carbamate ion pairs that bind with greater affinity than primary *n*-alkylamines. These observations indicate that carboxylic acids and phosphonic acids complicate the removal of carboxylate and phosphonate ligands using amines. Colloidal dispersions of CdSe[NH_2R] are aggregate at amine concentrations below 0.1 M, and the exchange of the amine ligands for tri-*n*-butylphosphine or tri-*n*-octylphosphine oxide also results in rapid nanocrystal aggregation, even in neat phosphine or molten phosphine oxide solution. Nanocrystals colloids solely stabilized by neutral donor ligands are relatively unstable compared to those stabilized electrostatically or by adsorption of metal carboxylates.

Introduction

Early strategies to exchange the ligands bound to cadmium selenide nanocrystals focused on neutral donors, such as tri-*n*-octylphosphine oxide (TOPO). However, more recent studies conclude that surface-bound metal carboxylate and phosphonate complexes or adsorbed ion pairs are the more dominant ligand types (*I*, Scheme 1).[1,2] Exchanging these ligands has required reagents that can cleave the metal carboxylate or metal phosphonate linkage, such trialkyloxonium salts,[3–6] or silyl and ammonium chalcogenides[7–9] and halides.[10–12] In most cases, these approaches produce electrostatically stabilized dispersions in polar solvents where a surface-bound cation or anion balances charge with an outersphere counter ion (*II*, Scheme 1). The surface-bound ions provide a valuable avenue to tailor nanocrystal properties, however the counter ions can lead to capacitive currents, low charge transport mobilities, and hysteretic transport properties.[14, 17,18, 18–21] Nonetheless, electrostatically stabilized nanocrystals have enabled rapid progress in the fabrication of nanocrystal photovoltaics and thin film transistors with record breaking efficiency gains in recent years.[19–21]

On the other hand, well-characterized nanocrystals solely stabilized by neutral ligands are rare. In many cases samples that were thought to be stabilized by neutral donors, including TOPO[22] and primary *n*-alkylamines,[26] turn out to be stabilized by impurities such as phosphonate and phosphinate anions, or *n*-alkylammonium-*N*-*n*-alkylcarbamate salts formed from primary amines and carbon dioxide (*III*, Scheme 1).[25]

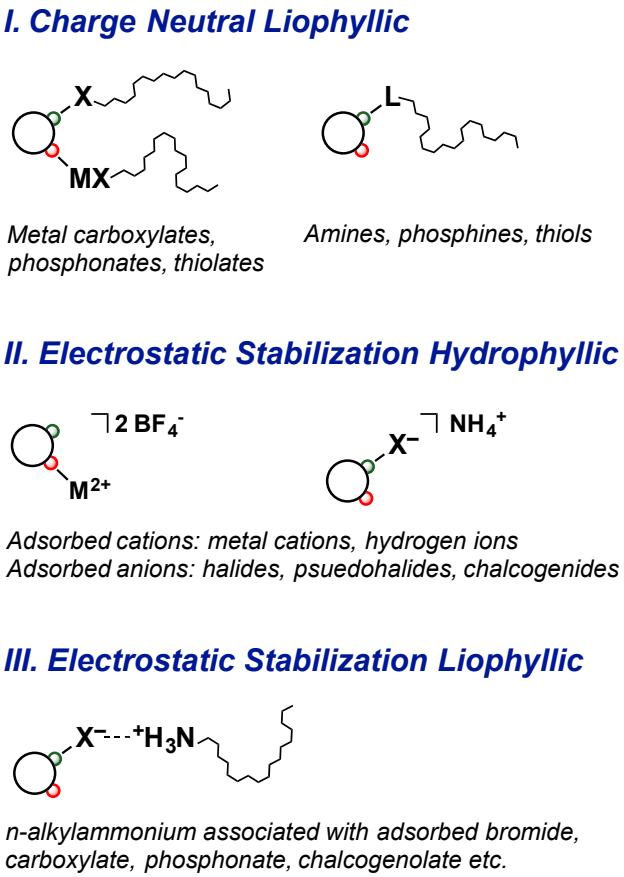

Scheme 1. Common modes of stabilizing a colloidal dispersion.

In principle, a nanocrystal bound solely by labile neutral donors could be obtained by completely displacing adsorbed anions or surface bound metal complexes using Lewis bases.[25] However, previous attempts to do so using *n*-alkylamines,[26,27] phosphines,[26,28] and pyridine[29–31] consistently report partial ligand exchange, with a small fraction (10-15%)[32] of the ligands proving difficult to remove.[33] Recent work on the displacement of cadmium carboxylate ligands from zinc blende cadmium selenide nanocrystals found that diamines and primary *n*-alkylamines are effective displacement reagents, removing as much as 90–95% of the ligand shell as measured *in situ* using ^{1}H nuclear magnetic resonance (NMR) spectroscopy. However, even

following repeated cycles of displacement and purification under optimized conditions, 3–10% of the starting carboxylate ligands remain.

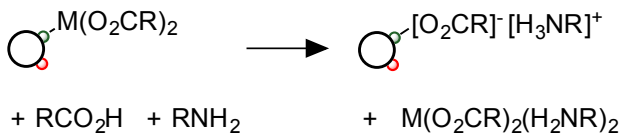

Scheme 2. Ion pair stabilization by nanocrystal surface.

Although the origin of the tightly bound fraction of carboxylate was unclear at the outset of our study, we reasoned that it resulted from an adsorbed ammonium carboxylate ion pair formed from an amine and a carboxylic acid rather than a metal carboxylate complex (*III*, Scheme 1). Our hypothesis arose from a recent study of ligand cleavage using trimethylsilyl chloride where protic impurities in the starting carboxylate terminated nanocrystals (CdSe–$Cd(O_2CR)_2$), led to the formation and adsorption of hydrochloride salts: tri-*n*-butylphosphonium chloride and *n*-butylammonium chloride.[10] The same protic impurities could also complicate the displacement of cadmium carboxylate. For example, addition of *n*-alkylamines to carboxylate terminated CdSe nanocrystals containing a carboxylic acid impurity (CdSe–$Cd(O_2CR)_2$/HO_2CR) could form *n*-alkylammonium and carboxylate ions that bind the nanocrystal (Scheme 2). If both ions remain inner sphere, it would be difficult to distinguish an adsorbed ammonium carboxylate ion pair from amine and cadmium carboxylate ligands. In principle, the adsorption of ammonium carboxylate and ammonium phosphonate salts can explain reports of partial ligand exchange when amines are used as displacement reagents provided that there affinity for the surface is strong. To test this hypothesis, we developed a method to scavenge carboxylic acids and other acidic impurities from CdSe–$Cd(O_2CR)_2$/HO_2CR using dimethylcadmium ($CdMe_2$) or

diethylzinc ($ZnEt_2$). With the acid free nanocrystals, we investigated the subsequent displacement of their $Cd(O_2CR)_2$ surface ligands and the reactivity of product amine bound nanocrystal CdSe–NH_2R.

Results and Discussion

Reaction of CdSe–$Cd(O_2CR)_2$/HO_2CR with $CdMe_2$. Addition of $CdMe_2$ to CdSe–$Cd(O_2CR)_2$/HO_2CR causes the immediate formation of methane (δ = 0.16 ppm) as observed *in situ* using ^{1}H NMR spectroscopy. After 24 hours, unreacted Me_2Cd can be removed under vacuum leaving nanocrystals with surface bound methyl groups CdSe–$Cd(O_2CR)_2$/$CdMe_2$ that are visible as a broad ^{1}H NMR resonance of low intensity in benzene-d_6 solution (δ = 0.4 ppm, 0.15 nm^{-2}, ~7 per nanocrystal, see below) (Figure 1). To the best of our knowledge, this is the first report of metal chalcogenide nanocrystals with metal-alkyl lignads.

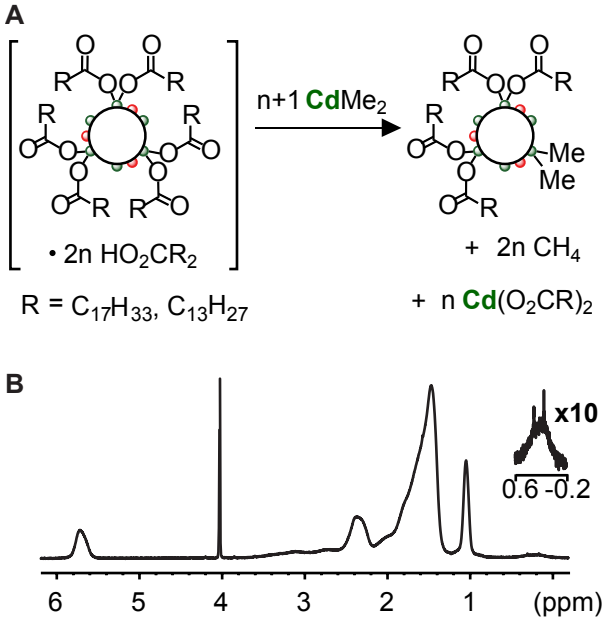

Figure 1. (**A**) Reaction of CdSe[$Cd(O_2CR)_2$/HO_2CR] with $CdMe_2$ methylates the nanocrystal surface. (**B**) ^{1}H NMR spectrum of the product nanocrystals showing resonances from carboxylate ligands, a ferrocene internal standard (δ = 4 ppm), as a well as a broad signal from surface bound methyl groups (δ = 0.4 ppm).

Interestingly, photolysis of CdSe–$Cd(O_2CR)_2$/$CdMe_2$ changes the UV-visible absorbance spectrum by reducing the extinction of the lowest excitonic transitions and quenching the photoluminescence (Figure 2). An intraband absorption feature appears in the infrared spectral range (ω = 2000–4000 cm^{-1}) that is characteristic of a nanocrystal containing electrons in its conduction band.[16,34–36] Exposure of the sample to air recovers the absorbance and photoluminescence properties of the starting CdSe–$Cd(O_2CR)_2$ verifying the reduction process is reversible (Figure S1). Related spectroscopic changes have been reported upon exposure of nanocrystals to triethylborohydride, sodium biphenyl, and other reductants.[35,37,38] Photolysis of CdSe–$Cd(O_2CR)_2$/$CdMe_2$ also eliminates the broad ^{1}H NMR signal from surface bound methyl groups and produces CH_4 (δ = 0.2 ppm) in benzene-d_6 and a mixture of CH_4 and CH_3D in tetrahydrofuran-d_8 solution (Figure S2-S3).# We conclude that the photoexcited nanocrystal oxidizes the surface bound methyl groups, eliminating methyl radicals that abstract a hydrogen or deuterium atom from the carboxylate ligands or the tetrahydrofuran-d_8 solvent.

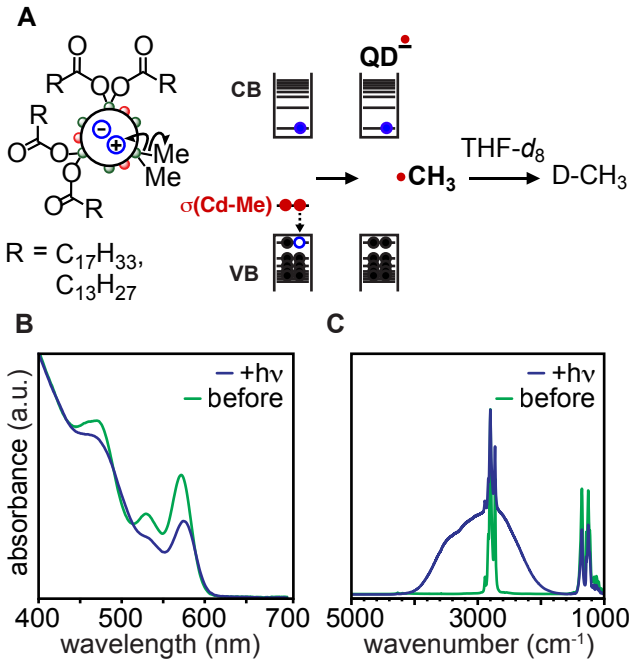

Figure 2. (**A**) Reaction scheme illustrating hole trapping at a Cd–Me bond and liberation of a methyl radical as well as an *n*-doped nanocrystal ($QD^{\bullet-}$). Hydrogen atom abstraction from the solvent produces CH_3D. (**B**) UV-Visible absorption spectra illustrating the change in the excitonic features before (green) and after (blue) photolysis. (**C**) Infrared absorption spectra before (green) and after (blue) photolysis showing an intraband absorption feature that is coincident with (C–H) stretching bands.

Reaction of CdSe–$Cd(O_2CR)_2$/HO_2CR with $ZnEt_2$. Addition of $ZnEt_2$ to CdSe–$Cd(O_2CR)_2$/HO_2CR leads to the immediate formation of ethane (δ = 0.8 ppm), however, no evidence of photochemical reduction of the nanocrystals and no NMR signals from surface bound ethyl groups are observed. After isolation of our Et_2Zn treated nanocrystals, no changes to the absorption spectrum could be observed other than a slight blue shift of the absorption onset (Figure S4). However, during the preparation of this manuscript a related study reported photochemical reduction of CdSe nanocrystals in the presence of $ZnEt_2$.[38] The origin of this discrepancy is uncertain, although the nanocrystals herein were synthesized by a different method. It is also worth noting that the $ZnEt_2$ used in our study was freshly distilled prior to use in order the avoid the accidental addition of metallic zinc.

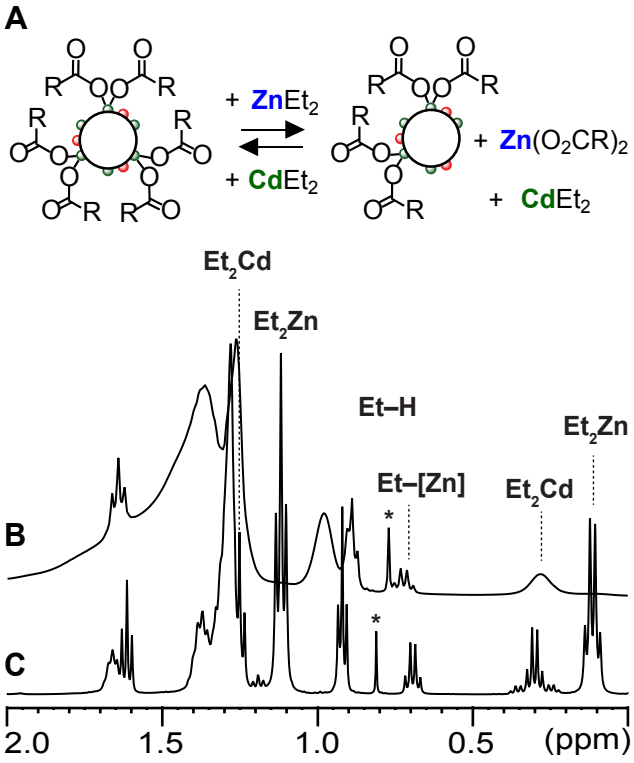

Figure 3. (**A**) Reaction of CdSe–$Cd(O_2CR)_2$/HO_2CR with $ZnEt_2$ leads to $CdEt_2$ and $Zn(O_2CR)_2$. (**B**) ^{1}H NMR spectrum of reaction between CdSe–$Cd(O_2CR)_2$/HO_2CR and $ZnEt_2$. (*) is assigned to ethane. Unlabeled signals are from carboxyl chains bound to the nanocrystal or free in solution. (**C**) ^{1}H NMR spectrum of the reaction between $Cd(O_2CR)_2$ and $ZnEt_2$. $^{111/113}$Cd satellites can be seen surrounding both signals from the methylene and the methyl groups of Et_2Cd (δ = 0.30 and 1.25 ppm).

Interestingly, addition of $ZnEt_2$ (2 equiv/carboxylate) induces desorption of ~50% of the carboxyl ligands and produces $CdEt_2$. In addition, a new quartet is visible that is upfield of typical aliphatic resonances (δ = 0.7–0.9 ppm), that we tentatively assign to the methylene resonance of a pentanuclear zinc cluster, $Zn_5Et_4(O_2CR)_6$, on the basis of its chemical shift and the lack of Cd satellites. An analogous structurally characterized cluster ($Zn_5Et_4(OAc)_6$) is a known to form upon conproportionation of zinc acetate and $ZnEt_2$. (http://pubs.acs.org/doi/pdf/10.1021/om900683z) An independent study of the reaction between $ZnEt_2$ and cadmium oleate also produces $CdEt_2$, which matches the chemical shift and $J_{Cd\text{-}H}$

couplings reported earlier (δ = 1.25 ppm, $^{3}J_{Cd\text{-}H}$ = 30 Hz, δ = 0.3 ppm, $^{2}J_{Cd\text{-}H}$ = 50 Hz).[39,40] After removal of the volatiles under vacuum and precipitation of the nanocrystals from toluene, zinc oleate can be recovered from the supernatant which was verified using Fourier transform infrared (FT-IR), ^{13}C NMR, ^{1}H NMR, and energy dispersive X-ray spectroscopies (Figure S5). These observations indicate that $ZnEt_2$ and $Cd(O_2CR)_2$ undergo metathesis to $CdEt_2$, $Zn(O_2CR)_2$, and a minor amount of $Zn_5Et_4(O_2CR)_6$. We conclude that conversion of $ZnEt_2$ to $Zn(O_2CR)_2$ causes the desorption of the carboxylate ligands, presumably because $Zn(O_2CR)_2$ has a weaker affinity for the cadmium selenide surface than does $Cd(O_2CR)_2$. The decreased carboxylate coverage helps explain the observed reduction in the PLQY from 10% to 2%.[25]

The small amounts of both ethane and methane that rapidly form upon adding $ZnEt_2$ or $CdMe_2$ to CdSe–$Cd(O_2CR)_2$/HO_2CR_2 support the presence of an impurity sufficiently acidic to rapidly protonolyze the Zn–Et or Cd–Et bond. Integrating the ^{1}H NMR signals from the ethane and methane byproducts indicates that the acidic impurity makes up 10 mol% of the ligand shell, a finding that is consistent with our previous study of ligand exchange using trimethylsilyl chloride.[10] We hypothesize that oleic acid present in the ligand shell is the source of these acidic hydrogens, (the presence of water was ruled in the previous study by the lack of a *bis*-trimethylsilylether coproduct) however a selenol or other protic impurity produced by the synthesis could also be involved.

Adsorption of Oleic Acid and Oleic Acid-d_1 to CdSe-$Cd(O_2CR)_2$

To investigate the binding of oleic acid to CdSe[$Cd(O_2CR)_2$] we added oleic acid to a sample of CdSe[$Cd(O_2CR)_2$] that had previously been reacted with Et_2Zn and had its $Cd(O_2CR)_2$ coverage reduced to 0.59 oleate nm^{-2} (see Experimental). The added oleic acid increases the

intensity of broad ^{1}H NMR signals characteristic of bound oleate ligands (Figure S6) and diffusion ordered spectroscopy measurements (DOSY, Figure S7) support the binding of oleic acid to the nanocrystal. However, a signal from the acidic hydrogen could not be identified. Five cycles of precipitation, centrifugation, and redissolution only partially reduce the oleate coverage to 1.14 oleate ligands nm^{-2}, or twice the initial coverage. Thus the ligand shell is composed of roughly 50% oleic acid and 50% oleate ligands in this case.

The FT-IR spectrum of CdSe[Cd(O_2CR)$_2$] after adsorbing oleic acid is indistinguishable from the starting CdSe[Cd(O_2CR)$_2$] with no carboxylic acid band (ν(C=O) = 1710 cm^{-1}) (Figure S8) and no signals from selenol (ν(Se–H) ~ 2300 cm^{-1})[41] or hydroxyl (ν(O–H) ~ 3000–4000 cm^{-1}) groups. Moreover, adsorption of oleic acid-d_1 (O–D) does not produce new FT-IR signals, nor were any signals visible in the difference spectrum after adsorption, however, inadequate background subtraction in the water region may obscure such a signal. The ^{2}H NMR spectrum of this compound is indistinguishable from that of an as synthesized CdSe[Cd(O_2CR)$_2$] sample (Figure S9). Addition of Et_2Zn to the nanocrystals, however, does result in the production of CH_2D–CH_3 confirming the presence of the deuterium label (Figure S9). While the location of the acidic hydrogen is uncertain, it is clear that added oleic acid adsorbs to the nanocrystal in significant quantities and is not easily separated by precipitation of the nanocrystals.

Having developed a procedure to remove acidic hydrogens from the nanocrystals, we were able to completely displace carboxylate from the surface producing nanocrystals with carboxylate coverages of < 0.1 nm^{-2} (Figure 4).[b] Attempts to completely remove Cd(O_2CR)$_2$ by repeated precipitation from concentrated *n*-octylamine solution (4.5 M) and prior to removing the acidic impurities only partially eliminates the carboxylate ligands (0.3 nm^{-2}), explaining our previous report.[25] We hypothesize that the formation of tightly adsorbed *n*-octylammonium

oleate ion pairs might explain the residual 0.3 oleates nm^{-2} that cannot be removed by repeated precipitation from amine solution. However, if CdSe[$Cd(O_2CR)_2/HO_2CR_2$] is first treated with Et_2Zn or Me_2Cd, $Cd(O_2CR)_2$ can be completely displaced from the surface.

Interestingly, ^{1}H NMR spectra of CdSe[$Cd(O_2CR)_2$] dissolved in *n*-octylamine (4.5 M) and toluene-d_8 show that as much as 90% of the oleate ligands are freely tumbling in the amine solution (Figure S10a).[c] However, nanocrystals precipitated from this mixture retain roughly 50% of their original coverage. Repeated precipitation of the nanocrystals from 4.5 M *n*-alkylamine solutions was required to completely separate *n*-butylamine and *n*-octylamine bound nanocrystals (CdSe[NH_2R], R = C_4H_9, C_8H_{17}) from cadmium carboxylate coproducts (see Supporting Information). Attempts to improve the efficiency of the precipitation process by varying the amine structure, solvent mixture, reaction time, concentration, *etc*. proved largely unsuccessful and will be described in detail elsewhere (Figure S10).

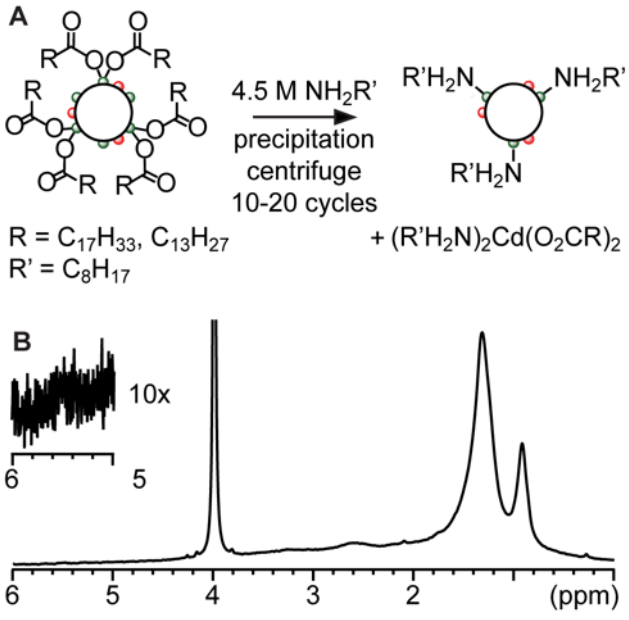

Figure 4. (**A**) Synthesis of CdSe[NH_2R] by displacement of $Cd(O_2CR)_2$ with primary amines. (**B**) ^{1}H NMR spectrum of CdSe[NH_2R]. The inset shows the lack of vinyl resonance from oleate ligands. The signal at $\delta = 4$ ppm is from ferrocene, which is used as an internal standard.

The amine ligands bound to $CdSe[NH_2R]$ are labile at room temperature, but effectively stabilize a colloidal dispersion provided that the amine concentration remains above 0.1 M.[d] Below 0.1 M the nanocrystals slowly precipitate, although the precipitate can be partially redispersed upon stirring in *n*-alkylamine solution at 60 °C. Transmission electron microscope (TEM) images of $CdSe[NH_2R]$ (R = *n*-butyl, *n*-hexyl, *n*-octyl) prepared from 0.1 M amine solution are disordered and aggregated regardless of the amine chain length (Figure S10). However, UV-Vis absorption and dynamic light scattering measurements on nanocrystal dispersions are consistent with unaggregated nanocrystals (Figures S13-14). Moreover, when $CdSe[NH_2R]$ is converted back to $CdSe[Cd(O_2CR)_2]$, monolayers of well separated nanocrystals can be obtained on TEM grids (Figure S15). We conclude that aggregation observed in the TEM images of $CdSe[NH_2R]$ is reversible and occurs upon drying the sample.

Given the propensity of $CdSe[NH_2R]$ to aggregate, we sought to test the stability of nanocrystal dispersions solely stabilized by 4-ethylpyridine, tri-*n*-butylphosphine (Bu_3P) or TOPO ligands. Dissolving $CdSe[NH_2R]$ in neat Bu_3P or 4-ethylpyridine at room temperature or in molten TOPO (50 °C) and stirring under dynamic vacuum induces slow precipitation of the nanocrystals over 30 minutes as the amine ligands desorb and evaporate. Neither 4-ethylpyridine, Bu_3P nor TOPO ligands stabilize a dispersion even under neat conditions (> 3 M). Compared to metal carboxylates, metal phosphonates, and ammonium chalcogenide and halide ion pairs, which provide stable dispersions at relatively low coverages, amines, phosphines, and phosphine oxides provide much weaker stabilization.

Formation and Binding of Ammonium Oleate. To study the binding of *n*-alkylammonium oleate ligands to the nanocrystal surface, oleic acid (1 equiv/amine) was added to $CdSe[NH_2R]$ ($R = C_8H_{17}$, Scheme 3). An FT-IR spectrum of this mixture showed asymmetric

and symmetric stretches from amine ligands as well as *n*-octylammonium ions (ν(N–H) = 3000–3700 cm^{-1}) (Figure 5A). A difference spectrum between the nanocrystals with *n*-octylammonium oleate and *n*-octylamine ligands, CdSe[NH_2R/($[O_2CR]^-[H_3NR]^+$] and CdSe[NH_2R] leaves a broad signal that we assign to stretching vibration from an *n*-octylammonium ion (ν(N–H) = 3250–3750 cm^{-1}). This band is higher in frequency than ν(O–H) from carboxylic acids and on the high end of the range expected for *n*-alkylammonium ions.[42] The stretching frequency suggests that the *n*-octylammonium ions in this sample are only weakly stabilized by hydrogen bonding, which typically reduces the stretching band energy.[43] In addition, carboxylate stretching bands are visible (ν(C–O) = 1408, 1564 cm^{-1}) that are distinct from the ν(N–H) of CdSe[NH_2R] (ν = 1417, 1558 cm^{-1}), oleic acid (ν = 1710 cm^{-1}),[44] or a mixture of oleic acid and CdSe[$Cd(O_2CR)_2$] (ν = 1435, 1536, 1749 cm^{-1}). Thus, the formation of *n*-octylammonium oleate can be assigned on the basis of its FT-IR spectrum, especially by the observation of the ν(N–H) stretching band.

With this spectroscopic handle in hand, we were curious if this alkylammonium oleate species could be observed in an as synthesized CdSe[$Cd(O_2CR)_2$] sample treated with octylamine. Upon treating a sample five times with a 4.5 M octylamine solution and reducing the ligand coverage to < 0.5 carboxylates nm^{-2} a broad stretching frequency centered around ~3400 cm^{-1} is clearly visible (Figure S16), indicating that at low carboxylate coverages these ion pairs can be observed. Thus, acidic impurities, while difficult or impossible to observe spectroscopically, are still present in typical nanocrystal samples.

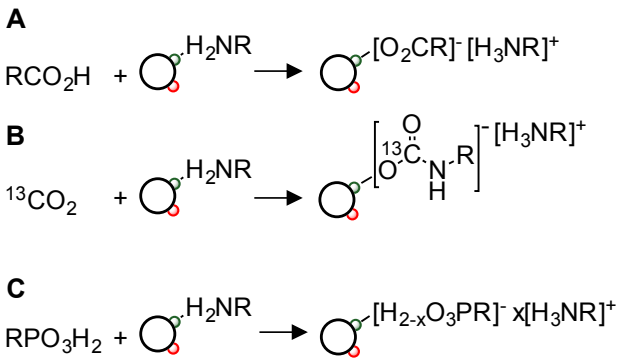

Scheme 3. Addition of acidic molecules to CdSe[NH_2R] leads to acid dissociation and the adsorption of an ion pair.

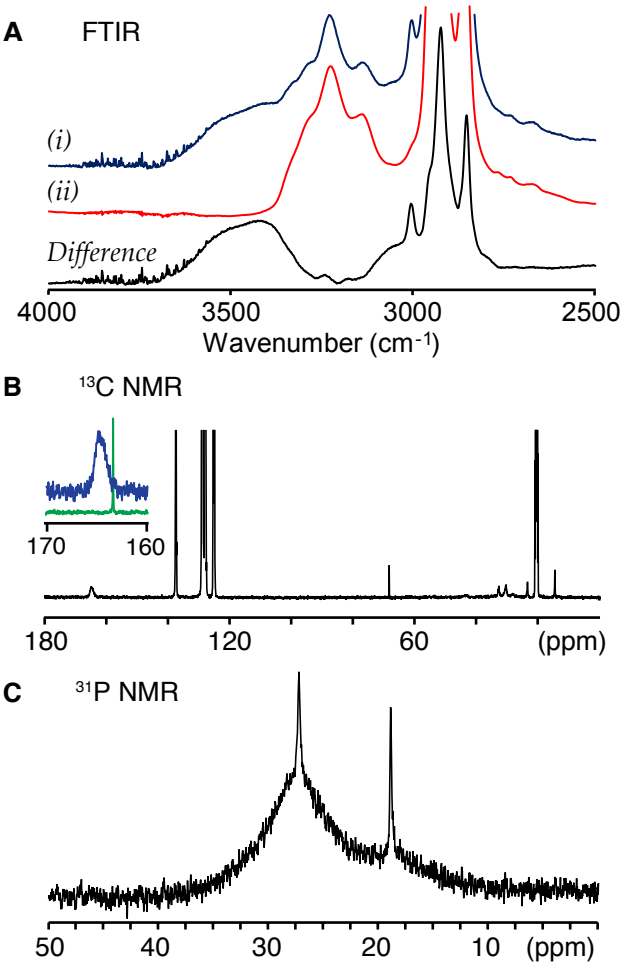

Figure 5. (A) FT-IR spectra of CdSe[NH_2R/$[O_2CR]^-[H_3NR]^+$] (R = C_8H_{17}), (*i*), CdSe[$NH_2C_8H_{17}$] (*ii*), and their difference spectrum (*iii*). (*i*) and (*ii*) are normalized by the absorbance maximum of

the amine ν(N–H) stretching band at 3200 cm^{-1}). (B) ^{13}C NMR spectrum of an isolated and purified sample of CdSe[$NH_2C_8H_{17}$] after exposure to $^{13}CO_2$ in a 0.04 M *n*-octylamine solution in toluene. The inset shows the region from 160–170 ppm where a broad resonance centered at 165 ppm corresponding to the carbamate carbon (blue) is visible. The signal is near the resonance of *n*-octylammonium N-*n*-octylcarbamate prepared in the absence of nanocrystals (green). (C) ^{31}P NMR spectrum of CdSe[$NH_2C_8H_{17}$] ([$NH_2C_8H_{17}$] = 0.021 M) and a stoichiometric amount of *n*-octadecylphosphonic acid. Sharp and broad signals are assigned to free and bound *n*-octadecylphosphonate anions, respectively.

In nonpolar solution, *n*-octylamine is not sufficiently basic to fully deprotonate a carboxylic acid as can be demonstrated using FT-IR spectroscopy.[45] However, in the presence of CdSe[$NH_2C_8H_{17}$], we observe that oleic acid is converted to surface bound *n*-octylammonium oleate (0.59 nm^{-2}, Figure 5A) . Presumably, binding of the oleate anion to the Lewis acidic cadmium selenide surface stabilizes its negative charge. A similar conclusion was reached in a study of metal oxide nanocrystals,[2,46] however, no ion pair formation was reported under similar conditions in a recent study of amine bound $CuInS_2$ nanocrystals.[47]

Considering the high concentration of amines in the experiments above, the binding of *n*-alkylammonium oleate ion pairs is strong. Even in 4.5 M *n*-alkylamine solution, surface bound *n*-alkylammonium oleate ligands are visible in the ^1H NMR spectrum. Moreover, the coverage of these ligands only drops from 0.59 nm^{-2} to 0.16 oleates per nm^2 after three cycles of precipitation from 4.5 M *n*-octylamine solution. These observations support an affinity that is much higher than primary *n*-alkylamines, a feature that may stem from their ability to chelate surface atoms, or positive charge density of zinc blende crystal facets. [e]

In order to test the generality of the ion pair formation and coordination, we exposed $CdSe[NH_2C_8H_{17}]$ to *n*-octadecylphosphonic acid and monitored the products using ^{31}P NMR spectroscopy (Scheme 3 and Figure 5). *n*-Octadecylphosphonic acid is sufficiently acidic to protonate *n*-alkylamines in the absence of nanocrystals.[48] Addition to $CdSe[NH_2C_8H_{17}]$ produces two broad ^{31}P NMR resonances that we assign to monohydrogen *n*-octadecylphosphonate (δ = 27.2 ppm) and *n*-octadecylphosphonate (δ = 18.8 ppm) on the basis of an independent titration experiment between *n*-octadecylphosphonic acid and *n*-octylamine (Figure S20). Again, the signal breadth shows that these species bind the nanocrystal even in 0.1 M amine solution. This relatively strong binding may also explain the difficulty of displacing native phosphonic acid ligands from nanocrystals using amine donors.[49–51]

Carbon dioxide reacts with $CdSe[NH_2C_8H_{17}]$ to form nanocrystals with *n*-octylammonium-*N*-*n*-octylcarbamate ligands, $CdSe[H_2NR/\ [O_2C–NHR]^-[H_3NR]^+]$ (Scheme 3 and Figure 5b). Upon adding labeled carbon dioxide-^{13}C to a solution of $CdSe[NH_2R]$, a broad ^{13}C NMR signal from the carbonyl carbon of a surface bound carbamate anion appears (δ = 165 ppm, $\Delta\delta$ = 1.95 ppm, 975 Hz). Integration of its ^{13}C NMR signal acquired using an inverse gated decoupling scheme and comparing it to a natural abundance ferrocene standard shows that ~ 0.1 carbamates nm^{-2} remain bound to the nanocrystal following one round of precipitation using methyl acetate. This coverage remains unchanged following three cycles of precipitation from concentrated *n*-octylamine solution (4.5 M).

The FT-IR spectrum of $CdSe[H_2NR/[O_2C–NHC_8H_{17}]^-[H_3NR]^+]$ shows signals from *n*-octylammonium and *N*-*n*-octylcarbamate ions including a band for the H_3NR^+ fragment (ν(N–H) = 3200 cm^{-1}, Figure S18), three bands (3028, 3064, and 3087 cm^{-1}) that appear in an authentic sample of *n*-octylammonium *N*-*n*-octylcarbamate, and an additional band (ν(-NCO_2^-) =

1496 cm^{-1}) corresponding to the antisymmetric stretch of the carbamate anion (Figure S21).[52] Liquid primary amines are known to dissolve significant quantities of carbon dioxide, leading to *n*-alkylammonium and *N*-*n*-alkylcarbamate ions that can dictate the outcome of syntheses that use amine surfactants.[23] Given how easily these species are formed in air and their relatively high affinity for the nanocrystal surfaces, $CdSe[NH_2R]$ must be stored free from air to avoid reaction with carbon dioxide and contamination of its ligand shell.

Among the modes of stabilizing a colloidal dispersion described in Scheme 1, the electric double layer formed by adsorbed ions pairs is perhaps most common. Sorption of ions on metal oxide surfaces in particular has been the subject of great interest for decades.[53–55] Colloidal dispersions of organic micelles and polymer beads in aqueous media share a similar motif where ions form an electric double layer arrangement.[56] Likewise, recent examples of metal chalcogenide, metal oxide, metal, and metal halide nanocrystals have been synthesized with chalcogenide, thiocyanate, halide, citrate, or other polyanionic surface ligands that balance their charge with an outer sphere counter ion and dissolve in polar media.[18,21,57–59] In the present case, however, we document examples where organic counter ions remain tightly paired with the nanocrystal surface and the nanocrystal ion pair complex remains soluble in non polar media such as toluene. While this mode of stabilization is well documented in the literature on metal nanocrystals where surfactants such as hexadecyltrimethylammonium bromide (CTAB) can stabilize dispersions of metal nanocrystals in toluene,[60] the experiments above indicate that the adsorption of ion pairs is difficult to avoid when utilizing amine surfactants. Moreover, it is a significant challenge to differentiate between adsorbed ions such as ammonium carboxylate or ammonium carbamate salts, and metal oleate and/or amine ligands.

While many have proposed that neutral donor ligands stabilize a colloidal dispersion of metal chalcogenide quantum dots, several observations made here indicate that neutral ligands provide relatively weak stabilization: (1) the tendency of $CdSe[NH_2R]$ to aggregate unless the concentration of amine is above 0.1 M, (2) the well known lability of amine ligands on the ^1H NMR timescale (~ms),[61] (3) the complete desorption of amines from nanocrystal thin films,[62] and (4) the instability of CdSe nanocrystals in neat pyridine, TOPO or Bu_3P solution described above. We can also conclude that metal carboxylate complexes, or adsorbed ammonium halide, carboxylate, or carbamate ion pairs bind the nanocrystals more strongly than do amines. Given the challenge of spectroscopically differentiating between an ammonium carboxylate ion pair and separate amine and carboxylate ligands, we conclude that the formation and binding of ion pairs are likely more pervasive than realized, especially in nanocrystals stabilized by primary aliphatic amines.

Conclusion

The deprotonation of acidic molecules such as carboxylic acids, phosphonic acids and carbamic acids, is facilitated by the Lewis acidic surface of CdSe nanocrystals. The surface tightly binds the resultant anionic carboxylate, phosphonate, and carbamate ions, and prevents the complete displacement of the native ligands with primary amines. To address this limitation, we used Et_2Zn and Me_2Cd to scavenge acidic hydrogens prior to displacing the surface metal oleate complexes. This strategy provides CdSe nanocrystals without anionic impurities, but the nanocrystals proved relatively unstable to aggregation unless the amine concentration was maintained above 0.1M. The stability worsens following exchange of the primary amine ligands for commonly used ligands such as pyridine, TOPO or Bu_3P. These experiments show the

somewhat surprising result that most neutral donor ligands do not effectively support stable colloidal dispersions. Moreover, it suggests that the stability of nanocrystals reported to be bound solely by neutral donor ligands, and amine ligands in particular, may benefit from the presence of impurities that provide electrostatic stabilization.

Experimental Section

General Methods: Cadmium nitrate tetraaquo (99%), sodium hydroxide, myristic acid (99%), selenium dioxide (99.8%), anhydrous oleic acid (99%), 1-tetradecanol (95%), tri-*n*-butylphosphine (99%), methanol (99.8%), $^{13}CO_2$ (99% atom enriched, 1L lecture bottle), deuterium chloride (35 wt. % in D_2O), 1-octadecene (90%) were purchased from Sigma Aldrich and used without further purification. Ferrocene (98%) was purchased from Sigma Aldrich and purified by sublimation before use. Tri-*n*-octylphosphine oxide (99%) was purchased from Sigma Aldrich and recrystallized from acetonitrile before use. Benzene-d_6 (99.6%), toluene-d_8 (99.5%), tetrahydrofuran-d_8 (99.5%), anhydrous acetonitrile (99.5%), anhydrous tetrachloroethylene (99%) and anhydrous methyl acetate (99.5%) were purchased from Sigma Aldrich, shaken with activated alumina, filtered, and stored over 4 Å molecular sieves in an inert atmosphere glovebox at least 24 hours prior to use. Pentane, tetrahydrofuran, and toluene were dried over alumina columns, shaken with activated alumina, filtered and stored over 4 Å molecular sieves in an inert atmosphere glovebox at least 24 hours prior to use. Dimethyl cadmium and diethyl zinc were purchased from Strem and vacuum distilled prior to use. *CAUTION: Me_2Cd is extremely toxic and because of its volatility and air sensitivity should only be handled by a highly trained and skilled researcher*. N,N,N′,N′-Tetramethylethylenediamine (TMEDA, 99.5%), 1,2-diaminocyclohexane (mixture of *cis* and *trans* isomers), *n*-Octylamine (99%), *n*-hexylamine, and *n*-butylamine were purchased from Sigma Aldrich and dried over CaH_2, distilled, and stored in a nitrogen glove box. *n*-octadecylphosphonic acid was synthesized as described previously.[63,64] Cadmium myristate and cadmium oleate were synthesized from $Cd(NO_3)_2{\cdot}4H_2O$ and the corresponding carboxylic acid on a 25 mmol scale following a modified procedure reported previously.[65]

All manipulations were performed under air free conditions unless otherwise indicated using standard Schlenk techniques or within a nitrogen atmosphere glove box. NMR spectra were recorded on Bruker Avance III 500 MHz instruments. ^{1}H NMR spectra were acquired with sufficient relaxation delay to allow complete relaxation between pulses (30 seconds). ^{31}P NMR spectra were recorded with 2 s delays between pulses. DOSY measurements were performed using a double stimulated echo sequence. The gradient strength was varied linearly from 2% to 95% of the probe's maximum value**.** The diffusion parameters consisting of the pulse length (δ/2) and delay (Δ) were chosen to ensure that > 90% of the signal decayed at the highest magnetic field gradient. UV-Visible data was obtained using a Perkin Elmer Lambda 950 spectrophotometer equipped with deuterium and tungsten halogen lamps. Photoluminescence spectra and quantum yields were measured using a FluoroMax-4 equipped with an Integrating Sphere from Horiba Scientific according to a previous report.[25] FT-IR spectra were obtained using either a sodium chloride or lithium fluoride liquid cell in tetrachloroethylene or a Harrick Praying Mantis sample holder for Diffuse Reflectance Infrared Fourier Transform Spectroscopy (DRIFTS) on a Thermo Scientific Nicolet 6700 spectrometer equipped with a liquid N_2 cooled MCT-A detector.

Synthesis of CdSe–Cd(O_2CR)$_2$. CdSe nanocrystals were synthesized using a previously reported procedure.[10,66] Purified nanocrystals without ^{1}H NMR signals from free oleyl chains were used to make stock solutions in benzene-d_6 ([$^{-}O_2$CR] = ~ 200 mM; [nanocrystal] = ~ 2 mM). These stock solutions were diluted 10-fold prior to NMR and 1000-fold prior to UV-visible absorption spectroscopy and PLQY measurements. The concentrations of nanocrystals and ligands in benzene-d_6 stock solutions were determined using a combination of NMR and UV-Visible absorption spectroscopies according to a previous report.[25] A stock solution of ferrocene (10–25 μL, 0.05 M) was added to a known volume of nanocrystal stock solution and the ferrocene signal used as an internal concentration standard.

Reaction of CdSe–Cd(O_2CR)$_2$ with Me_2Cd or Et_2Zn. Me_2Cd or Et_2Zn were added (1.7 mg Me_2Cd, or 1.9 mg Et_2Zn) using a microliter syringe to a CdSe stock solution (5 mL) and the solution protected from light. The solution was stirred for 12 hours and distilled to dryness under vacuum to remove unreacted Me_2Cd or Et_2Zn. The residue was dissolved in toluene (5 mL) and methyl acetate (40 mL) was added to precipitate the nanocrystals, which were isolated by centrifugation and decanting the supernatent. The precipitation and centrifiguation process was repeated twice and the final nanocrystal powder dried under vacuum before being dissolved in benzene-d_6 for ^{1}H NMR and UV-visible absorption analysis.

Reduction of cadmium carboxylate coverage with TMEDA. Reduction of the cadmium carboxylate coverage in CdSe–Cd(O_2CR)$_2$ nanocrystal samples was done following a previously reported method.[25,67] In a typical reaction, CdSe–Cd(O_2CR)$_2$ that was previously reacted with Et_2Zn according to **Reaction of CdSe–Cd(O_2CR)$_2$ with Me_2Cd or Et_2Zn** was dissolved in 5 mL of neat TMEDA and allowed to stir for 10 minutes. The solution was then precipitated with 25 mL of methyl acetate and the nanocrystals isolated by centrifugation. The clear supernatant was discarded and the pellet subjected to two additional cycles of TMEDA/methylacetate/centrifugation. The nanocrystals were then separated from adventitious TEMDA by two cycles of dissolution in toluene (5 mL), precipitation with methyl acetate (25 mL), and centrifugation. The resulting nanocrystals were insoluble in pentane but could be redispersed in toluene or benzene.

Binding of oleic acid to CdSe–Cd(O_2CR)$_2$ with reduced oleate coverage. In a typical reaction, a stock solution of CdSe–Cd(O_2CR)$_2$ (500 μL, [nanocrystals] = 0.48 mM, [Cd(O_2CR)$_2$] = 0.013 M, 0.53 carboxylates nm^{-2}) that had previously been treated with TMEDA according to **Reduction of cadmium carboxylate coverage with TMEDA** in either benzene-d_6 or tetrachloroethylene, was added oleic acid (12 μL, 394 equiv. per nanocrystal) and solution allowed to stir for 3 hours. The nanocrystals were then precipitated by adding methyl acetate (10mL) and isolated by centrifugation.

The red pellet was then purified by five cycles of dissolution in pentane (1 mL), precipitation with methyl acetate (10 mL), and centrifugation. The nanocrystals were then dispersed in benzene-d_6 for NMR spectroscopy.

Synthesis of CdSe–NH_2R (R = $C_{12}H_{25}$, C_8H_{17}, C_4H_9). A solution of *n*-octylamine in toluene (5 mL, 4.5 M) was added to a stock solution of CdSe nanocrystals (2 mL, [$Cd(O_2CR)_2$] = 0.1 M) and the red solution stirred for 10 minutes. Methyl acetate (25mL) was added and the precipitate isolated by centrifugation. This process was repeated 10-fold or until no vinyl resonance was visible in the ^{1}H NMR spectrum. After the final centrifugation the nanocrystals were dissolved in toluene, dried under vacuum, and characterized by NMR and UV-visible absorption spectroscopies (see above). If partial precipitation of nanocrystals occurs, 20 μL of primary amine was added to the nanocrystals to aid in redissolution. The photoluminescence quantum yield of isolated CdSe–NH_2R is 1–2%. *n*-Octylamine ligands were exchanged for *n*-butyl- or n-dodecylamine by three rounds of dissolation/precipitation/centriguation procedure from a 1 M solution of the desired alkylamine in toluene.

Digestion of CdSe–$NH_2C_8H_{17}$. The volatiles were removed from a stock solution of CdSe–$NH_2C_8H_{17}$ (500 μL, [nanocrystal] = 0.5–2.3 mM, [$NH_2C_8H_{17}$] = 0.2–0.3 M) under vacuum over 48 hours (this ensures removal of the majority of the octylamine species). Under an argon atmosphere, a 1 mL solution of DCl (2.8 mmol) in a D_2O and methanol-d_4 (1:1 by volume) was added to this residue. The sample was shaken to mix its components and the mixture gradually dissolved to a clear solution and was left standing overnight. The next day, a colorless solution was obtained, to which pyridine (10 μL) was added as an internal concentration standard for ^{1}H NMR analysis. The number of aliphatic chains from species other than *n*-octylammonium was estimated by from the difference between the integral of the methyl resonance, which measures all aliphatic chains groups, and the integral of the α-CH_2 from *n*-octylammonium. Due to the trace amount of organic impurities in these

samples, a high concentration of the nanocrystal stock solution is required. Under our conditions, signal to noise ratios of the methyl resonance ranged from 100:1–1000:1.

Replacement of *n*-octylamine ligands with cadmium oleate. A solution of CdSe–$NH_2C_8H_{17}$ ([nanocrystals] = 2.26 mM) was dried under vacuum for three hours to remove the volatiles. To this residue, cadmium oleate dissolved in toluene (2 mL, 0.165 M) was added. The resulting solution was allowed to stir overnight at room temperature, and then was purified by precipitation with 10 mL of methyl acetate and centrifugation, affording a red powder that was redissolved in toluene prior to analysis with TEM.

Reaction of oleic acid and CdSe–$NH_2C_8H_{17}$. A stock solution of CdSe–$NH_2C_8H_{17}$ was diluted with a solution of oleic acid in benzene-d_6 ([nanocrystal] = .135 mM, [$NH_2C_8H_{17}$] = 24 mM, [RCO_2H] = 240 mM) and the sample was allowed to sit overnight. The nanocrystals were then purified by three cycles of precipitation with methyl acetate (5 mL), centrifugation, and redissolution. The nanocrystal pellet then dissolved in pentane (5mL) transferred to a 20 mL vial fitted with a stir bar and placed under vacuum to remove the volatiles. The final nanocrystal powder was dissolved in 1 mL benzene-d_6 or ^{1}H NMR and UV-visible absorption analysis. Attempts to displace surface bound *n*-octylammonium oleate using *n*-octylamine followed three cycles of precipitation from 4.5 M amine solution according to the procedure described in the section titled **Synthesis of CdSe–NH_2R**.

Reaction of n-octadecylphosphonic acid and CdSe–$NH_2C_8H_{17}$. To a solution of CdSe-$NH_2C_8H_{17}$ (600 μL, [nanocrystals] = 0.12 mM, [amine] = 21 mM) in a J-Young tube was added 4.28 mg (12.3 μmoles) of *n*-octadecylphosphonic acid. The mixture was sonicated to aid the dissolution of the phosphonic acid and then allowed to react overnight prior to analysis with ^{31}P NMR spectroscopy.

Reaction of carbon dioxide and CdSe–$NH_2C_8H_{17}$. A solution of CdSe-$NH_2C_8H_{17}$ in toluene-d_8 (600 μL, [nanocrystals] = 0.24 mM, [amine] = 42.7 mM) was placed in a J-Young tube and degassed. Meanwhile, the gas manifold of a Schlenk line was filled with carbon dioxide obtained from the sublimation of dry ice. Carbon dioxide was then admitted to a volumetric gas addition bulb (209 mL) until the internal pressure was 10 torr as measured with a mercury monometer. This volume of gas was then condensed into the J-Young tube at liquid nitrogen temperature for 5 minutes, The J-Young tube was then sealed and allowed to warm to room temperature. Addition of isotopically enriched $^{13}CO_2$ (10 μmoles) to CdSe-$NH_2C_8H_{17}$ was performed identically to the procedure described above using a lecture bottle of ^{13}C-labeled carbon dioxide. After standing for 4 hours at room temperature methyl acetate (10 mL) was added and the nanocrystal precipitate isolated by centrifugation. The isolated nanocrystals were further purified by three cycles of dissolution in toluene, precipitation with methyl acetate, and centrifugation.

SUPPORTING INFORMATION Additional reaction schemes, ^{1}H NMR and UV-Vis absorption spectra of selected nanocrystal samples and control experiments, example ^{1}H NMR spectra of digested nanocrystal samples, DOSY, comparisons of different cleaning methods, TEM images, and DLS measurements are included free of charge via the Internet at http://pubs.acs.org.

ACKNOWLEDGMENT This work was funded by the Department of Energy under Grant No. DE-SC0006410. NCA and PEC acknowledge support from the National Science Foundation under Grants No. DGE07-07425 and No. DGE11-44155, respectively. The authors also thank Columbia University for support. Ilan Jen-La Plante is acknowledged for her TEM work, which was conducted at the New York Structural Biology Center constructed with support from Research Facilities Improvement Program Grant number C06 RR017528-01-CEM from the National Center for Research Resources, National Institutes of Health.

REFERENCES

(1) Owen, J. The Coordination Chemistry of Nanocrystal Surfaces. *Science.* **2015**, *347* (6222), 615–616.

(2) De Roo, J.; Justo, Y.; De Keukeleere, K.; Van den Broeck, F.; Martins, J. C.; Van Driessche, I.; Hens, Z. Carboxylic-Acid-Passivated Metal Oxide Nanocrystals: Ligand Exchange Characteristics of a New Binding Motif. *Angew. Chemie Int. Ed.* **2015**, *54* (22), 6488–6491.

(3) Doris, S. E.; Lynch, J. J.; Li, C.; Wills, A. W.; Urban, J. J.; Helms, B. a. Mechanistic Insight into the Formation of Cationic Naked Nanocrystals Generated under Equilibrium Control. *J. Am. Chem. Soc.* **2014**, *136* (44), 15702–15710.

(4) Rosen, E. L.; Buonsanti, R.; Llordes, A.; Sawvel, A. M.; Milliron, D. J.; Helms, B. A. Exceptionally Mild Reactive Stripping of Native Ligands from Nanocrystal Surfaces by Using Meerwein's Salt. *Angew. Chemie Int. Ed.* **2012**, *51* (3), 684–689.

(5) Caldwell, M. A.; Albers, A. E.; Levy, S. C.; Pick, T. E.; Cohen, B. E.; Helms, B. A.; Milliron, D. J. Driving Oxygen Coordinated Ligand Exchange at Nanocrystal Surfaces Using Trialkylsilylated Chalcogenides. *Chem. Commun.* **2011**, *47* (1), 556–558.

(6) Dong, A.; Ye, X.; Chen, J.; Kang, Y.; Gordon, T.; Kikkawa, J. M.; Murray, C. B. A Generalized Ligand-Exchange Strategy Enabling Sequential Surface Functionalization of Colloidal Nanocrystals. *J. Am. Chem. Soc.* **2011**, *133* (4), 998–1006.

(7) Hughes, B. K.; Ruddy, D. A..; Blackburn, J. L.; Smith, D. K.; Bergren, M. R.; Nozik, A. J.; Johnson, J. C.; Beard, M. C. Control of PbSe Quantum Dot Surface Chemistry and Photophysics Using an Alkylselenide Ligand. *ACS Nano* **2012**, *6* (6), 5498–5506.

(8) Kim, D. K.; Fafarman, A. T.; Diroll, B. T.; Chan, S. H.; Gordon, T. R.; Murray, C. B.;

Kagan, C. R. Solution-Based Stoichiometric Control over Charge Transport in Nanocrystalline CdSe Devices. *ACS Nano* **2013**, *7* (10), 8760–8770.

(9) Turo, M. J.; Macdonald, J. E. Crystal-Bound vs Surface-Bound Thiols on Nanocrystals. *ACS Nano* **2014**, *8* (10), 10205–10213.

(10) Anderson, N. C.; Owen, J. S. Soluble, Chloride-Terminated CdSe Nanocrystals: Ligand Exchange Monitored by 1 H and 31 P NMR Spectroscopy. *Chem. Mater.* **2013**, *25* (1), 69–76.

(11) Zhang, H.; Jang, J.; Liu, W.; Talapin, D. V. Colloidal Nanocrystals with Inorganic Halide, Pseudohalide, and Halometallate Ligands. *ACS Nano* **2014**, *8* (7), 7359–7369.

(12) Tang, J.; Kemp, K. W.; Hoogland, S.; Jeong, K. S.; Liu, H.; Levina, L.; Furukawa, M.; Wang, X.; Debnath, R.; Cha, D.; Chou, K. W.; Fischer, A.; Amassian, A.; Asbury, J. B.; Sargent, E. H. Colloidal-Quantum-Dot Photovoltaics Using Atomic-Ligand Passivation. *Nat. Mater.* **2011**, *10* (10), 765–771.

(13) Nag, A.; Kovalenko, M. V; Lee, J.; Liu, W.; Spokoyny, B.; Talapin, D. V. Metal-Free Inorganic Ligands for Colloidal Nanocrystals: S^{2-}, HS^{-}, Se^{2-}, HSe^{-}, Te^{2-}, HTe^{-}, TeS_3^{2-}, OH^{-}, and NH_2^{-} as Surface Ligands. *J. Am. Chem. Soc.* **2011**, *133* (27), 10612–10620.

(14) Oh, S. J.; Berry, N. E.; Choi, J. H.; Gaulding, E. A.; Paik, T.; Hong, S. H.; Murray, C. B.; Kagan, C. R. Stoichiometric Control of Lead Chalcogenide Nanocrystal Solids to Enhance Their Electronic and Optoelectronic Device Performance. *ACS Nano* **2013**, *7* (3), 2413–2421.

(15) Liu, Y.; Tolentino, J.; Gibbs, M.; Ihly, R.; Perkins, C. L.; Liu, Y.; Crawford, N.; Hemminger, J. C.; Law, M. PbSe Quantum Dot Field-Effect Transistors with Air-Stable Electron Mobilities above 7 $cm^2\ V^{-1}\ S^{-1}$. *Nano Lett.* **2013**, *13* (4), 1578–1587.

(16) Wehrenberg, B. L.; Guyot-Sionnest, P. Electron and Hole Injection in PbSe Quantum Dot Films. *J. Am. Chem. Soc.* **2003**, *125* (26), 7806–7807.

(17) Nag, A.; Chung, D. S.; Dolzhnikov, D. S.; Dimitrijevic, N. M.; Chattopadhyay, S.; Shibata, T.; Talapin, D. V. Effect of Metal Ions on Photoluminescence, Charge Transport, Magnetic and Catalytic Properties of All-Inorganic Colloidal Nanocrystals and Nanocrystal Solids. *J. Am. Chem. Soc.* **2012**, *134* (33), 13604–13615.

(18) Dirin, D. N.; Dreyfuss, S.; Bodnarchuk, M. I.; Nedelcu, G.; Papagiorgis, P.; Itskos, G.; Kovalenko, M. V. Lead Halide Perovskites and Other Metal Halide Complexes As Inorganic Capping Ligands for Colloidal Nanocrystals. *J. Am. Chem. Soc.* **2014**, *136* (18), 6550–6553.

(19) Kovalenko, M. V.; Manna, L.; Cabot, A.; Hens, Z.; Talapin, D. V.; Kagan, C. R.; Klimov, V. I.; Rogach, A. L.; Reiss, P.; Milliron, D. J.; Guyot-Sionnnest, P.; Konstantatos, G.; Parak, W. J.; Hyeon, T.; Korgel, B. A.; Murray, C. B.; Heiss, W. Prospects of Nanoscience with Nanocrystals. *ACS Nano* **2015**, *9* (2), 1012–1057.

(20) Talapin, D. V.; Lee, J.-S.; Kovalenko, M. V.; Shevchenko, E. V. Prospects of Colloidal Nanocsrystals for Electronic and Optoelectronic Applications. *Chem. Rev.* **2010**, *110*, 389–458.

(21) Fafarman, A. T.; Koh, W. K.; Diroll, B. T.; Kim, D. K.; Ko, D. K.; Oh, S. J.; Ye, X.; Doan-Nguyen, V.; Crump, M. R.; Reifsnyder, D. C.; Murray, C. B.; Kagan, C. R. Thiocyanate-Capped Nanocrystal Colloids: Vibrational Reporter of Surface Chemistry and Solution-Based Route to Enhanced Coupling in Nanocrystal Solids. *J. Am. Chem. Soc.* **2011**, *133* (39), 15753–15761.

(22) Wang, F.; Tang, R.; Buhro, W. E. The Trouble with TOPO; Identification of Adventitious

Impurities Beneficial to the Growth of Cadmium Selenide Quantum Dots, Rods, and Wires. *Nano Lett.* **2008**, *8* (10), 3521–3524.

(23) Belman, N.; Israelachvili, J. N.; Li, Y.; Safinya, C. R.; Bernstein, J.; Golan, Y. Reaction of Alkylamine Surfactants with Carbon Dioxide: Relevance to Nanocrystal Synthesis. *Nano Lett.* **2009**, *9* (5), 2088–2093.

(24) Luo, B.; Rossini, J. E.; Gladfelter, W. L. Zinc Oxide Nanocrystals Stabilized by Alkylammonium Alkylcarbamates. *Langmuir* **2009**, *25* (22), 13133–13141.

(25) Anderson, N. C.; Hendricks, M. P.; Choi, J. J.; Owen, J. S. Ligand Exchange and the Stoichiometry of Metal Chalcogenide Nanocrystals: Spectroscopic Observation of Facile Metal-Carboxylate Displacement and Binding. *J. Am. Chem. Soc.* **2013**, *135* (49), 18536–18548.

(26) Kim, W.; Lim, S. J.; Jung, S.; Shin, S. K. Binary Amine-Phosphine Passivation of Surface Traps on CdSe Nanocrystals. *J. Phys. Chem. C* **2010**, *114* (3), 1539–1546.

(27) Lefrançois, A.; Couderc, E.; Faure-Vincent, J.; Sadki, S.; Pron, A.; Reiss, P. Effect of the Treatment with (Di-)Amines and Dithiols on the Spectroscopic, Electrochemical and Electrical Properties of CdSe Nanocrystals' Thin Films. *J. Mater. Chem.* **2011**, *21* (31), 11524-11531.

(28) Hanrath, T.; Veldman, D.; Choi, J. J.; Christova, C. G.; Wienk, M. M.; Janssen, R. a J. PbSe Nanocrystal Network Formation during Pyridine Ligand Displacement. *ACS Appl. Mater. Interfaces* **2009**, *1* (2), 244–250.

(29) Zillner, E.; Fengler, S.; Niyamakom, P.; Rauscher, F.; Köhler, K.; Dittrich, T. Role of Ligand Exchange at CdSe Quantum Dot Layers for Charge Separation. *J. Phys. Chem. C* **2012**, *116* (31), 16747–16754.

(30) Ji, X.; Copenhaver, D.; Sichmeller, C.; Peng, X. Ligand Bonding and Dynamics on Colloidal Nanocrystals at Room Temperature: The Case of Alkylamines on CdSe Nanocrystals. *J. Am. Chem. Soc.* **2008**, *130* (17), 5726–5735.

(31) Yu, D. N-Type Conducting CdSe Nanocrystal Solids. *Science.* **2003**, *300* (5623), 1277–1280.

(32) Kuno, M.; Lee, J. K.; Dabbousi, B. O.; Mikulec, F. V; Bawendi, M. G. The Band Edge Luminescence of Surface Modified CdSe Nanocrystallites : Probing the Luminescing State The Band Edge Luminescence of Surface Modified CdSe Nanocrystallites : Probing the Luminescing State. *J. Chem. Phys.* **1997**, *106* (23), 9869–9882.

(33) Donakowski, M. D.; Godbe, J. M.; Sknepnek, R.; Knowles, K. E.; Olvera de la Cruz, M.; Weiss, E. A. A Quantitative Description of the Binding Equilibria of Para-Substituted Aniline Ligands and CdSe Quantum Dots. *J. Phys. Chem. C* **2010**, *114* (51), 22526–22534.

(34) Guyot-Sionnest, P.; Wehrenberg, B.; Yu, D. Intraband Relaxation in CdSe Nanocrystals and the Strong Influence of the Surface Ligands. *J. Chem. Phys.* **2005**, *123* (7), 74709.

(35) Rinehart, J. D.; Schimpf, A. M.; Weaver, A. L.; Cohn, A. W.; Gamelin, D. R. Photochemical Electronic Doping of Colloidal CdSe Nanocrystals. *J. Am. Chem. Soc.* **2013**, *135* (50), 18782–18785.

(36) Schimpf, A. M.; Knowles, K. E.; Carroll, G. M.; Gamelin, D. R. Electronic Doping and Redox-Potential Tuning in Colloidal Semiconductor Nanocrystals. *Acc. Chem. Res.* **2015**, *48* (7), 1929–1937.

(37) Shim, M.; Guyot-Sionnest, P. N-Type Colloidal Semiconductor Nanocrystals. *Nature* **2000**, *407* (6807), 981–983.

(38) Tsui, E. Y.; Hartstein, K. H.; Gamelin, D. R. Selenium Redox Reactivity on Colloidal CdSe Quantum Dot Surfaces. *J. Am. Chem. Soc.* **2016**, *138* (35), 11105–11108.

(39) Tang, H.; Richey, H. G. Reactions of Diorganocadmium Compounds with Other Dialkylmetal Compounds and Macrocycles: Synthesis of Organocadmate Anions. *Organometallics* **2001**, *20* (8), 1569–1574.

(40) Turner, C. J.; White, R. F. Heteronuclear Magnetic Double-Resonance Studies of ^{113}Cd Shielding in Dialkyl Cadmium Compounds. *J. Magn. Reson.* **1977**, *26* (1), 1–5.

(41) Sharghi, N.; Lalezari, I. The Infrared Absorption Spectra of Selenomercaptans and Selenols. *Spectrochim. Acta* **1964**, *20* (2), 237–238.

(42) Waddington, T. C. 881. Infrared Spectra, Structure, and Hydrogen-Bonding in Ammonium Salts. *J. Chem. Soc.* **1958**, No. 4340, 4340.

(43) Miller, F. a; Wilkins, C. H. Infrared Spectra and Characteristic Frequencies of Inorganic Ions. *Anal. Chem.* **1952**, *24* (8), 1253–1294.

(44) Cox, B. G. *Acids and Bases: Solvent Effects on Acid-Base Strength*; Oxford University Press, 2013.

(45) Barrow, G. M.; Yerger, E. A. Acid-Base Reactions in Non-Dissociating Solvents. Acetic Acid and Triethylamine in Carbon Tetrachloride and Chloroform. *J. Am. Chem. Soc.* **1954**, *76* (20), 5211–5216.

(46) De Roo, J.; Van den Broeck, F.; De Keukeleere, K.; Martins, J. C.; Van Driessche, I.; Hens, Z. Unravelling the Surface Chemistry of Metal Oxide Nanocrystals, the Role of Acids and Bases. *J. Am. Chem. Soc.* **2014**, *136* (27), 9650–9657.

(47) Dierick, R.; Van den Broeck, F.; De Nolf, K.; Zhao, Q.; Vantomme, A.; Martins, J. C.; Hens, Z. Surface Chemistry of CuInS 2 Colloidal Nanocrystals, Tight Binding of L-Type

Ligands. *Chem. Mater.* **2014**, *26* (20), 5950–5957.

(48) Demmer, C. S.; Krogsgaard-Larsen, N.; Bunch, L. Review on Modern Advances of Chemical Methods for the Introduction of a Phosphonic Acid Group. *Chem. Rev.* **2011**, *111* (12), 7981–8006.

(49) Wang, F.; Tang, R.; Kao, J. L. F.; Dingman, S. D.; Buhro, W. E. Spectroscopic Identification of Tri-N-Octylphosphine Oxide (TOPO) Impurities and Elucidation of Their Roles in Cadmium Selenide Quantum-Wire Growth. *J. Am. Chem. Soc.* **2009**, *131* (13), 4983–4994.

(50) Owen, J. S.; Park, J.; Trudeau, P.-E.; Alivisatos, a. P. Reaction Chemistry and Ligand Exchange at Cadmium-Selenide Nanocrystal Surfaces. *J. Am. Chem. Soc.* **2008**, *130* (37), 12279–12281.

(51) Gomes, R.; Hassinen, A.; Szczygiel, A.; Zhao, Q.; Vantomme, A.; Martins, J. C.; Hens, Z. Binding of Phosphonic Acids to CdSe Quantum Dots: A Solution NMR Study. *J. Phys. Chem. Lett.* **2011**, *2* (3), 145–152.

(52) Frasco, D. L. Infrared Spectra of Ammonium Carbamate and Deuteroammonium Carbamate. *J. Chem. Phys.* **1964**, *41* (7), 2134.

(53) Brown, G. E.; Henrich, V. E.; Casey, W. H.; Clark, D. L.; Felmy, A.; Goodman, D. W.; Gra, M.; Fe, Ä. P.; Maciel, G.; Mccarthy, M. I.; Nealson, K. H.; Sverjensky, D. A.; Toney, M. F.; Zachara, J. M. Metal Oxide Surfaces and Their Interactions with Aqueous Solutions and Microbial Organisms. **1999**, *1998*.

(54) Westall, J.; Hohl, H. A Comparison of Electrostatic Models for the Oxide/solution Interface. *Adv. Colloid Interface Sci.* **1980**, *12* (4), 265–294.

(55) Haworth, A. A Review of the Modelling of Sorption from Aqueous Solution. *Adv. Colloid*

Interface Sci. **1990**, *32* (1), 43–78.

(56) Hansen, J.; Löwen, H. Effective Interactions Between Electric Double Layers. *Annu. Rev. Phys. Chem.* **2000**, *51* (1), 209–242.

(57) Dolzhnikov, D. S.; Zhang, H.; Jang, J.; Son, J. S.; Panthani, M. G.; Shibata, T.; Chattopadhyay, S.; Talapin, D. V. Composition-Matched Molecular "solders" for Semiconductors. *Science (80-.).* **2015**, *347* (6220), 425–428.

(58) Kovalenko, M. V; Scheele, M.; Talapin, D. V. Colloidal Nanocrystals with Molecular Metal Chalcogenide Surface Ligands. *Science* **2009**, *324* (5933), 1417–1420.

(59) De Roo, J.; Ibáñez, M.; Geiregat, P.; Nedelcu, G.; Walravens, W.; Maes, J.; Martins, J. C.; Van Driessche, I.; Kovalenko, M. V.; Hens, Z. Highly Dynamic Ligand Binding and Light Absorption Coefficient of Cesium Lead Bromide Perovskite Nanocrystals. *ACS Nano* **2016**, *10* (2), 2071–2081.

(60) Cheng, W.; Dong, S.; Wang, E. Synthesis and Self-Assembly of Cetyltrimethylammonium Bromide-Capped Gold Nanoparticles. *Langmuir* **2003**, *19* (22), 9434–9439.

(61) Valdez, C. N.; Schimpf, A. M.; Gamelin, D. R.; Mayer, J. M. Low Capping Group Surface Density on Zinc Oxide Nanocrystals. *ACS Nano* **2014**, *8* (9), 9463–9470.

(62) Norman, Z. M.; Anderson, N. C.; Owen, J. S. Electrical Transport and Grain Growth in Solution-Cast, Chloride-Terminated Cadmium Selenide Nanocrystal Thin Films. *ACS Nano* **2014**, No. 7, 7513–7521.

(63) Anderson, N. C. The Surface Chemistry of Metal Chalcogenide Nanocrystals, Columbia University, 2014.

(64) Kosolapoff, G. M. Isomerization of Alkylphosphites. III. The Synthesis of N-Alkylphosphonic Acids. *J. Am. Chem. Soc.* **1945**, *67* (7), 1180–1182.

(65) Chen, O.; Chen, X.; Yang, Y.; Lynch, J.; Wu, H.; Zhuang, J.; Cao, Y. C. Synthesis of Metal-Selenide Nanocrystals Using Selenium Dioxide as the Selenium Precursor. *Angew. Chem. Int. Ed. Engl.* **2008**, *47* (45), 8638–8641.

(66) Hassinen, A.; Moreels, I.; de Mello Donegá, C.; Martins, J. C.; Hens, Z. Nuclear Magnetic Resonance Spectroscopy Demonstrating Dynamic Stabilization of CdSe Quantum Dots by Alkylamines. *J. Phys. Chem. Lett.* **2010**, *1* (17), 2577–2581.

(67) Busby, E.; Anderson, N. C.; Owen, J. S.; Sfeir, M. Y. Effect of Surface Stoichiometry on Blinking and Hole Trapping Dynamics in CdSe Nanocrystals. *J. Phys. Chem. C* **2015**, *119* (49), 27797–27803.

(a) Photolysis of CdSe–$Cd(O_2CR)_2$/$CdMe_2$ also induces the precipitation of a grey powder, that is assumed to be cadmium metal

(b) Digestion of CdSe–NH_2R in DCl/CD_3OD verified the absence of carboxylic acid ligands, although other organic fragments derived from C18 chains were isolated and characterized by mass spectrometry. 1–3 of these impurities per nanocrystal are present in the isolated product (Figure S11) that may result from side reactions between SeO_2 and ocatdecene during the precursor conversion.

(c) This displacement of only 75% of the cadmium carboxylate is in contrast to our previously reported results where these amine concentrations should displace >95% of the cadmium carboxylate from the nanocrystal surface. We propose that this discrepancy is due to a higher concentration of nanocrystals and cadmium carboxylate in this report relative to these past results (whereas we previously performed these *in situ* ^{1}H NMR studies with a carboxylate concentration of .02 M, these samples had a concentration of 0.1 M).

(d) Typical [nanocrystal] used in this study are 2–5 mM, corresponding to 50–125 amines per nanocrystal at [amine] = 0.1M, or ~3 amines nm^{-2}.

(e) The remaining *n*-octylammonium oleate ligands could be removed by adding excess Et_2Zn (Figure S17). In this case, a slight blue shift in the UV-Vis absorption and the formation of Et_2Cd (Figure S18, S19) were observed, indicating cation exchange between Cd^{2+} and Zn^{2+} in the nanocrystal. The different reactivity, compared to what is observed with CdSe-$Cd(O_2CR)_2/HO_2CR$, may result from polymeric zinc amides that form in a side reaction between *n*-octylamine and Et_2Zn.

(f) The other skeletal vibrations of the carbamate anion cannot be seen due to N-H and C-H bending modes of the amine ligands

A Library of Selenourea Precursors to PbSe Nanocrystals with Size Distributions Near the Homogeneous Limit

Michael P. Campos,[†] Mark P. Hendricks,[†] Alexander N. Beecher,[†] Robert A. Swain,[†] Gregory T. Cleveland,[†] Matthew Y. Sfeir,[‡] and Jonathan S. Owen[*,†]

[†]Department of Chemistry, Columbia University, New York, New York 10027, United States

[‡]Center for Functional Nanomaterials, Brookhaven National Laboratory, Upton, New York 11973, United States

ABSTRACT: We report a tunable library of N,N,N'-trisubstituted selenourea precursors and their reaction with lead oleate at 60–150 °C to form carboxylate-terminated PbSe nanocrystals in quantitative yields. Single exponential conversion kinetics can be tailored over four orders of magnitude by adjusting the selenourea structure. The wide range of conversion reactivity allows the extent of nucleation ([nanocrystal] = 4.6–56.7 μM) and the size following complete precursor conversion (d = 1.7–6.6 nm) to be controlled. Narrow size distributions (σ = 0.5–2%) are obtained whose spectral linewidths are dominated (73–83%) by the intrinsic single particle spectral broadening, as observed using spectral hole burning measurements. The intrinsic broadening decreases with increasing size (FWHM = 320–65 meV, d = 1.6–4.4 nm) that derives from exciton fine structure and exciton-phonon coupling rather than broadening caused by the size distribution.

INTRODUCTION

Lead selenide (PbSe) nanocrystals have shown several highly desirable optoelectronic properties including efficient multiple exciton generation in photovoltaic devices[1-3] and the assembly of square and honeycomb lattices with topological states and Dirac cones in their band structure.[1-6] These lattices have potential to display unprecedented electrical transport behavior provided that disorder from the nanocrystal size distribution can be reduced.[7] However, it has proven challenging to synthesize PbSe nanocrystals from conventional nanocrystal precursors such as tri-*n*-alkylphosphine selenides, which are relatively unreactive toward lead carboxylate. Low yields of PbSe (< 3%) are typically formed from more reactive secondary phosphine impurities in the tri-*n*-alkylphosphine starting material.[8,9] More recently, diphenylphosphine selenide,[9,10] *bis*(trimethylsilyl)selenide,[11] and other additives such as hexadecanediol[12] have been used to boost the conversion reactivity and improve the yield, but size control, and in particular, a high-yielding synthesis of PbSe nanocrystals relevant for photovoltaic cells (d < 3.9 nm, E_g > 1.0 eV), is needed.

In order to address the lack of selenium reagents with reactivity appropriate for the synthesis of PbSe, we developed a library of N,N,N'-trisubstituted selenoureas. The conversion reactivity of these precursors can be tailored by adjusting their substitution pattern, as we recently demonstrated using a library of analogous thioureas.[13] This tunable reactivity allows the rate of solute supply and the concentration of nanocrystals formed during nucleation to be adjusted[14-17] and the final size following complete precursor conversion to be controlled. Herein we report optimized precursors and conditions for the synthesis of PbSe nanocrystals across a broad range of sizes and at large scale. Narrow size distributions are obtained whose absorption spectral linewidths are dominated by the intrinsic single-particle line broadening rather than heterogeneous broadening caused by the size distribution. These narrow distributions reveal a decreasing single particle spectral linewidth as the size of the nanocrystal increases.

RESULTS AND DISCUSSION

Di- and trisubstituted selenoureas can be synthesized from isoselenocyanates, LiAlSeH, NaHSe, $(Me_2Al)_2Se$, N-heterocyclic carbenes, carbon diselenide, and Woollins' Reagent ($[PhP(Se)(\mu\text{-}Se)]_2$),[18] but these approaches can be complicated because key reagents or intermediates are unstable or must be prepared in multiple steps. However, a few disubstituted selenoureas have been prepared in a single step from alkyl isocyanides, elemental selenium, and primary amines.[19-22] We have greatly expanded this approach to prepare a library of di- and trisubstituted selenoureas **1**–**31** in 60–98% yields (Table 1). Unlike thioureas, tri- and di- substituted selenoureas are air-sensitive,[23] and in some cases slightly light-sensitive, eventually depositing elemental selenium over several months if stored under ambient conditions. Selenoureas are therefore best handled in the absence of air and stored in the dark, where they are indefinitely stable.

Scheme 1. Synthesis of N,N'-disubstituted and N,N,N'-trisubstituted selenoureas.

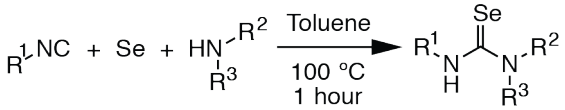

Table 1. Library of selenoureas.

	R^1	R^2	R^3	Yield (%)
1	*n*-C_4H_9	^{i}Pr	^{i}Pr	94
2	*n*-C_4H_9	–$(CH_2)_5$–		95
3	*n*-C_4H_9	*n*-C_4H_9	*n*-C_4H_9	97
4	*n*-C_4H_9	Et	Et	94
5	*n*-C_4H_9	*n*-C_4H_9	Me	98
6	*n*-C_4H_9	Allyl	Allyl	97
7	*n*-C_4H_9	Me	Me	88
8	*n*-C_4H_9	–$(CH_2)_4$–		68[a]
9	*n*-C_4H_9	4-MeO-Ph	Me	72[c]
10	Cy	*n*-$C_{12}H_{25}$	H	90[b]
11	Cy	Cy	Cy	65
12	Cy	^{i}Pr	^{i}Pr	57
13	Cy	^{i}Pr	Et	79
14	Cy	^{i}Pr	Me	90
15	Cy	–$(CH_2)_5$–		82
16	Cy	*n*-C_4H_9	*n*-C_4H_9	76
17	Cy	Et	Et	84
18	Cy	Et	Me	69
19	Cy	2-Me-$(CH_2)_4$–		88
20	Cy	tetrahydroisoquinolyl		95
21	Cy	Allyl	Allyl	98
22	Cy	Me	Me	76[a]
23	Cy	–$(CH_2)_4$–		89
24	Cy	4-MeO-Ph	Me	71
25	Cy	Ph	Me	64[d]
26	Cy	4-Cl-Ph	Me	27[e]
27	*n*-$C_{16}H_{33}$	^{i}Pr	Me	76
28	*n*-$C_{16}H_{33}$	Allyl	Allyl	63
29	*n*-$C_{16}H_{33}$	Ph	Me	73
30	^{t}Bu	Me	Me	72
31	^{t}Bu	–$(CH_2)_4$–		68

Reactions performed on 3 mmol scale for 1 hour unless otherwise noted. [a] Performed on 6.6 mmol scale. [b] Performed on 10 mmol scale. [c] 1.5 hour reaction time. [d] 2 hour reaction time. [e] 3 hour reaction time.

Table 2. Conversion of alkyl isoselenocyanates in the presence of N-methylanilines (entries 1–4) and dialkylamines (entries 5-6) determined by ^{77}Se NMR spectroscopy.

	R^1	R^2	R^3	Time (h)	Conv. (%)
1	*n*-C_4H_9	4-MeO-Ph	Me	1.5	>99
2	*n*-C_4H_9	Ph	Me	2	85
3	*n*-C_4H_9	4-Cl-Ph	Me	3	80
4	*n*-C_4H_9	4-CN-Ph	Me	8	< 1
5	*n*-C_4H_9	*n*-C_4H_9	*n*-C_4H_9	0.5	>99
6	Cy	Cy	Cy	0.5	87

Isocyanides react with elemental selenium at 100 °C in toluene to produce isoselenocyanates that are trapped by a variety of nucleophilic amines to form di- and trisubstituted selenoureas. Formation of the selenourea is conveniently monitored by ^{77}Se nuclear magnetic resonance (NMR) spectroscopy, where the chemical shifts of alkyl isoselenocyanates (δ = -345–-358 ppm)[24] and selenoureas (δ = 175–290 ppm) are distinct (Figure S1). In most cases, the isoselenocyanate does not accumulate and the rate of selenourea formation is limited by the dissolution of elemental selenium, which typically reaches completion over the course of one hour if 100 mesh selenium powder is used. However, less nucleophilic amines are slower to react and an isoselenocyanate intermediate can be observed. For example, while *n*-butylisoselenocyanate reacts quantitatively with electron-rich 4-methoxy-N-methylaniline to form **9** within 35 minutes, the analogous reaction with N-methylaniline proved more sluggish, requiring more than 2 hours to reach completion. Even more electron deficient 4-cyano-N-methylaniline proved unreactive toward *n*-butylisoselenocyanate over 8 hours (Table 2). Sterically bulky derivatives such as N,N,N'-tricyclohexylselenourea (**2**) can also be prepared in good yields provided that the amine trapping agent is sufficiently basic.

Most selenoureas in Table 1 are readily purified by recrystallization and could be structurally characterized using single crystal X-ray diffraction analysis (Figure S2). These structures reveal planar nitrogen atoms, an average C–Se bond length of 1.873 Å, and an average ∠NCN bond angle of 117.2° (Table S1). In all cases, a hydrogen atom was identified on the nitrogen atom and the C–Se bond length fell within the range typical of double bonds. Both features support the selone tautomer, as has been observed in other selenoureas.[25]

While N,N'-disubstituted thioureas are appropriately reactive for PbS nanocrystal synthesis,[13] analogous N,N'-disubstituted selenoureas (**10**) are too reactive, producing mixing limited kinetics upon injection into lead oleate solution at relatively low temperatures (80 °C). N,N,N'-Trisubstituted selenoureas provide slower, controllable conversion reactivity up to 150 °C. Tetrasubstituted selenoureas such as N,N,N',N'-tetramethylselenourea, on the other hand, are not reactive enough to produce soluble PbSe nanocrystals even at relatively high temperature (150 °C). Thus, much like was observed with thioureas, increasing the number of substituents decreases the reactivity toward lead oleate.

PbSe nanocrystals are synthesized by injection of N,N,N'-trisubstituted selenoureas dissolved in diphenyl ether, diglyme, or dibutyl ether into a solution of lead oleate in alkane or 1-alkene solvent at 60–150 °C (Figure 1A, S3). The formation of a deep red/brown color occurs 1–50 seconds following the injection, the timing of which depends on the selenourea structure. Monitoring the UV-Vis-NIR spectra of aliquots taken from the reaction mixture shows an increase in the concentration of PbSe and an increase in the average nanocrystal size (Figure S4). Depending on the selenourea structure and temperature, the reaction reaches completion and the nanocrystals approach their final size between 30 seconds (**12**) and 3 hours (**9**) following the injection. Optimization of the reaction temperature led to a convenient synthesis temperature of 100 °C where the conversion reactivity is controlled and does not suffer from mixing-limited kinetics. Reaction temperatures below 100 °C can lead to broader spectral linewidths. A reac

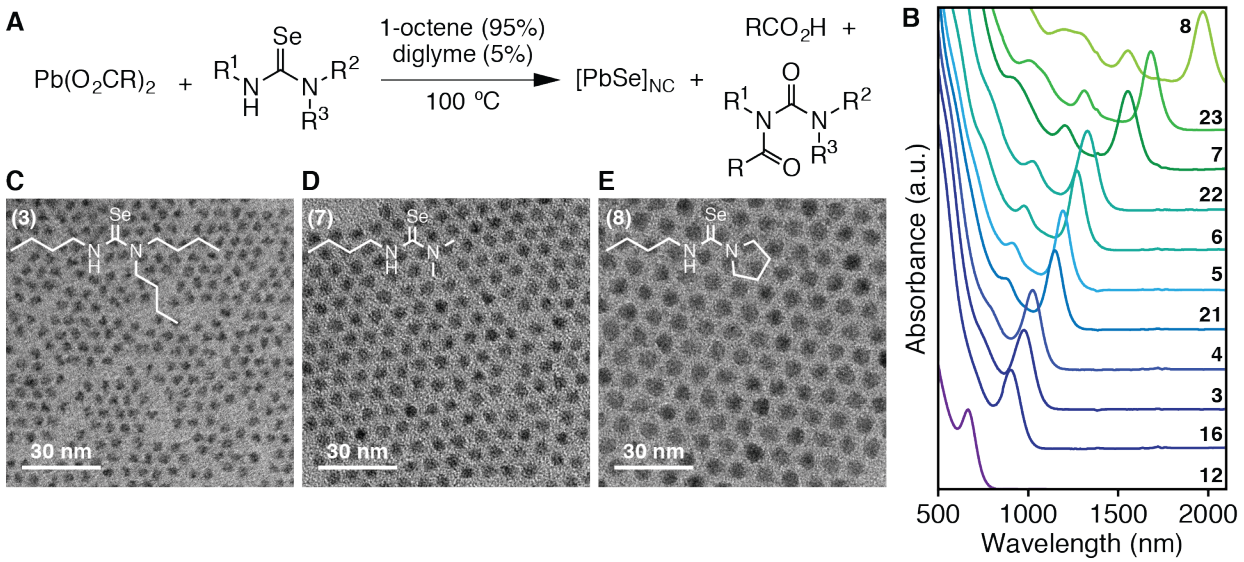

Figure 1. A) Reaction scheme for the synthesis of PbSe nanocrystals. B) UV-vis-NIR absorption spectra of aliquots removed from PbSe nanocrystal synthesis reactions at completion using the indicated precursors. C-E) Transmission electron micrographs of PbSe nanocrystals synthesized from **3**, **7**, and **8**. R = $C_{17}H_{33}$; R^1, R^2, R^3 = alkyl, aryl.

tion temperature of 100 °C is considerably lower than typically used to prepare PbSe from trioctylphosphine selenide (150–180 °C)[26,27] and within the range of temperatures used to synthesize PbSe from secondary phosphine selenide precursors (80–135°C).[9,10]

The structure of the selenourea reliably dictates the precursor reactivity and the nanocrystal size following complete conversion. The library of structures allows a wide range of nanocrystal sizes to be synthesized (d = 1.7–6.6 nm, $\lambda_{max}(1S_e–1S_h)$ = 615–2000 nm) with linewidths indicative of a narrow distribution of sizes (Figures 1B, S5). The full-width at half-maximum (FWHM) of the $1S_e–1S_h$ transition ranges from 35–350 meV and decreases with increasing nanocrystal size (Figures 1B, 4A). At larger sizes (d > 3.9 nm, E_g < 1.0 eV), these spectral linewidths are comparable to the best reported literature spectra,[28,29] but the smaller nanocrystals synthesized using selenoureas (d < 3.9 nm, E_g > 1.0 eV), including those that have band gaps relevant for solar cells (E_g > 1.2 eV), have much narrower linewidths than previous reports (Figure 4A). In the case of more reactive precursors **1** and **11**–**15,** unusually small nanocrystals were obtained (d = 1.6–2.9 nm, E_g = 1.3–2.1 eV) with spectral linewidths narrower than any previous example.[30-32]

The kinetics of PbSe formation were monitored *in situ* using a dip probe to measure the absorbance at λ = 400 nm.[13] At this wavelength the absorbance does not depend on the nanocrystal size and is proportional to the concentration of crystalline PbSe units.[8] Using ^{1}H NMR spectroscopy, clean conversion of the selenourea to the corresponding N-acylurea and oleic acid co-products is observed (Figure 1A, S6). The kinetics of the conversion reaction match the formation of PbSe measured using absorption spectroscopy (Figure S7). Thus, as was concluded in previous studies of PbS,[13] CdSe,[16] CdS,[33] and CdTe,[34] the precursor conversion kinetics can be indirectly monitored by the appearance of the nanocrystal absorption. Example UV-Vis absorption kinetics are shown in Figure 2B where the formation of PbSe approaches completion over the course of several minutes to an hour. Following a short induction period preceding crystal nucleation (1–50 sec), the evolution of the absorbance at 400 nm is well-described by a single exponential function (Figure 2C, S8) from which we extract a rate constant (k_{obs}, sec^{-1}).

By normalizing the k_{obs} to the slowest precursor (**26**), a series of relative conversion rate constants (k_{rel}) are obtained that can be used to assess the effect of the thiourea structure on the conversion reactivity (see Methods). For example, increasing the steric bulk of the substituents increases the k_{rel} over more than three orders of magnitude (Figure 2C). A similar increase in reactivity of thioureas with steric bulk suggests that elimination of lead sulfide and selenide from a chalcogenoureate complex may be involved in the rate determining step.[13] It is interesting to note that pyrrolidine-derived selenoureas are relatively unreactive compared to di-*n*-alkyl derivatives. We attribute the decreased reactivity to the more acute C–N–C substituent bond angle of the five-membered pyrrolidine ring (**23**, Figure S2L), which lowers its steric encumbrance. Consistent with this hypothesis, the analogous selenourea derived from piperidine (**15**, Figure S2D) has a wider C–N–C angle within the ring and converts at a faster rate. Aryl-substituted selenoureas (**24**–**26**, **9**) react an order of magnitude more slowly than their alkyl analogues (**18**, **22**). Similarly, N,N,N'-trisubstituted *thioureas* with aryl substituents are less reactive toward cadmium oleate than the aliphatic analogues.[13] However, aryl substituents *increase* the reactivity of N,N'-disubstituted thioureas toward lead oleate, where deprotonation or nucleophilic attack at the central carbon are thought to limit the rate of conversion.[13] On the other hand, the greater reactivity of electron-rich and bulky N,N,N'-trisubstituted selenoureas suggests that the conversion may be limited by unimolecular elimination of the metal chalcogenide.

Following the nucleation mass balance described by Sugimoto,[15] the number of nanocrystals produced by nucleation (n_f, L^{-1}) is determined by the solute supply rate (Q_o, mol L^{-1} s^{-1}) and the nucleus growth rate (vn, nm^3 L^{-1} s^{-1}), where V_m is the molar volume (nm^3 mol^{-1}) of a PbSe crystal monomer (Eq. 1).

$$n_f = \frac{Q_o V_m}{v_n} \quad (1)$$

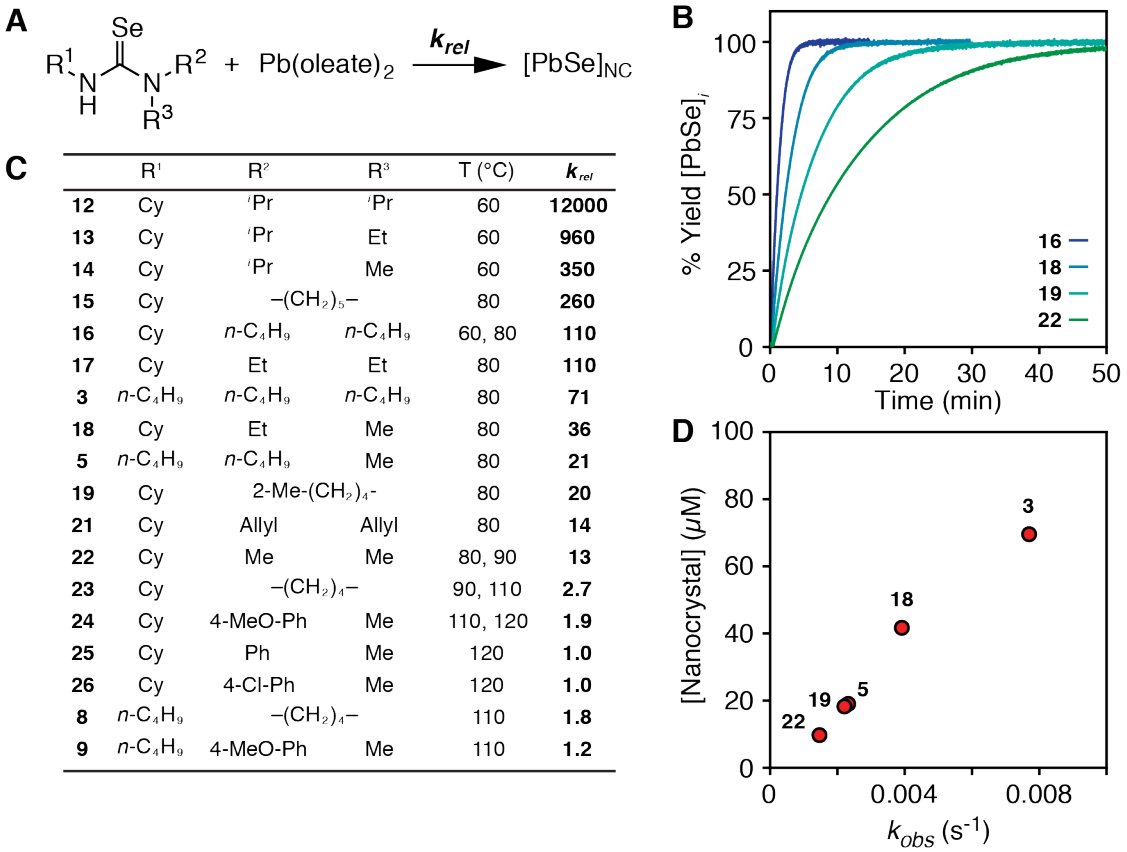

C

	R¹	R²	R³	T (°C)	k_{rel}
12	Cy	^{i}Pr	^{i}Pr	60	**12000**
13	Cy	^{i}Pr	Et	60	**960**
14	Cy	^{i}Pr	Me	60	**350**
15	Cy	–$(CH_2)_5$–		80	**260**
16	Cy	n-C_4H_9	n-C_4H_9	60, 80	**110**
17	Cy	Et	Et	80	**110**
3	n-C_4H_9	n-C_4H_9	n-C_4H_9	80	**71**
18	Cy	Et	Me	80	**36**
5	n-C_4H_9	n-C_4H_9	Me	80	**21**
19	Cy	2-Me-$(CH_2)_4$-		80	**20**
21	Cy	Allyl	Allyl	80	**14**
22	Cy	Me	Me	80, 90	**13**
23	Cy	–$(CH_2)_4$–		90, 110	**2.7**
24	Cy	4-MeO-Ph	Me	110, 120	**1.9**
25	Cy	Ph	Me	120	**1.0**
26	Cy	4-Cl-Ph	Me	120	**1.0**
8	n-C_4H_9	–$(CH_2)_4$–		110	**1.8**
9	n-C_4H_9	4-MeO-Ph	Me	110	**1.2**

Figure 2. A) Kinetic studies of PbSe formation from the reaction of lead oleate and selenoureas at 60–120 °C. B) Kinetics of PbSe formation as measured *in situ* by the absorbance at λ = 400 nm. C) Effect of structural changes on the relative single exponential rate constants (k_{rel}(**12**) to k_{rel}(**8**), e.g., k_{rel}(**24**) = k(**24**)/k(**26**)) of selenourea conversion. The wide range of reactivity requires that kinetics are measured at multiple temperatures. To account for the temperature dependence of the conversion rate constant, **16** and **22**–**24** were measured at two temperatures, and the change in rate constant was used to normalize the relative rate constants of the respective temperatures (e.g. k_{rel}(**8**) = [k(**8**)$^{110°C}$/k(**24**)$^{110°C}$] x [k(**24**)$^{120°C}$/k(**26**)$^{120°C}$]. D) Nanocrystal concentration versus rate constant (k_{obs}) of PbSe formation at 80 ° for **3**, **5**, **18**, **19**, and **22**. Reported k values are averages of three trials.

Consistent with this theory and previous studies of AgCl,[15] AgBr,[14] CdSe,[16,17] CdS,[13] and PbS,[13] we find that faster selenourea conversion kinetics result in larger n_f and smaller final nanocrystal sizes. This correlation is caused by changes to the extent of nucleation and is not affected by Ostwald ripening, which is negligibly slow under our conditions (Figure S9). The k_{obs} values extracted from PbSe formation kinetics are plotted versus the resultant nanocrystal concentrations in Figure 2D, where a linear correlation between the conversion reactivity and the nanocrystal concentration can be observed. From the slope of the plot we extract a nucleus growth rate v_n of 0.94 PbSe units/sec according to Eq. 1. Using this growth rate and the size distributions extracted below, we estimate the length of the nucleation period to be on the order of 3–16 seconds.

The library of conversion reactivity also allows the reaction temperature and precursor to be independently optimized to obtain a desired result. For example, by choosing the appropriate precursor, mixing-limited kinetics during the injection are avoided at large reaction scales (1–5 grams) (Figures 3B, S10, 11). This allowed us to develop a large scale synthesis of nanocrystals with a band gap appropriate for the fabrication of photovoltaic devices (λ_{max}($1S_e$–$1S_h$) = 985–1015 nm). Moreover, low-boiling solvents (b.p.(1-octene) = 122 °C; b.p.(Bu_2O) = 142 °C; b.p.(diglyme) = 162 °C, respectively) can be chosen that are then easily distilled from the crude nanocrystal product, facilitating the isolation process on large scale. Complete conversion of the starting materials leaves a final reaction mixture whose composition is defined by the starting ratios of reactants, thereby allowing a standard purification procedure to be developed that reproducibly produces nanocrystals with a known ligand coverage (Table S2, Figure S12). Optimized isolation procedures that provide reproducible chemical compositions are especially important in light of the reversible surface passivation provided by metal carboxylates, which bind the nanocrystal and influences the photoexcited carrier recombination.[35,36]

The size distribution of colloidal nanocrystals is often estimated by analyzing the spectral linewidth of the first optical transition. However, this analysis typically assumes the intrinsic linewidth of a single size is much lower than broadening caused by the size distribution.[33,37,38] Recent measurements suggest that exciton-phonon coupling, spectral diffusion, and exciton fine structure can account for more than 50% of the room temperature ensemble linewidth in highly monodisperse samples, which is at odds with the aforementioned assumption.[39-41] Moreover, photoluminescence correlation measurements on CdSe quantum dots[40] and the absorption spectra of atomically precise CdSe clusters[42] show a decreasing intrinsic linewidth as the size increases. Thus, in samples of colloidal crystals with narrow size distributions the spectral linewidth of the ensem-

ble depends on both the intrinsic linewidth of single particles, the particle size, and the size distribution.

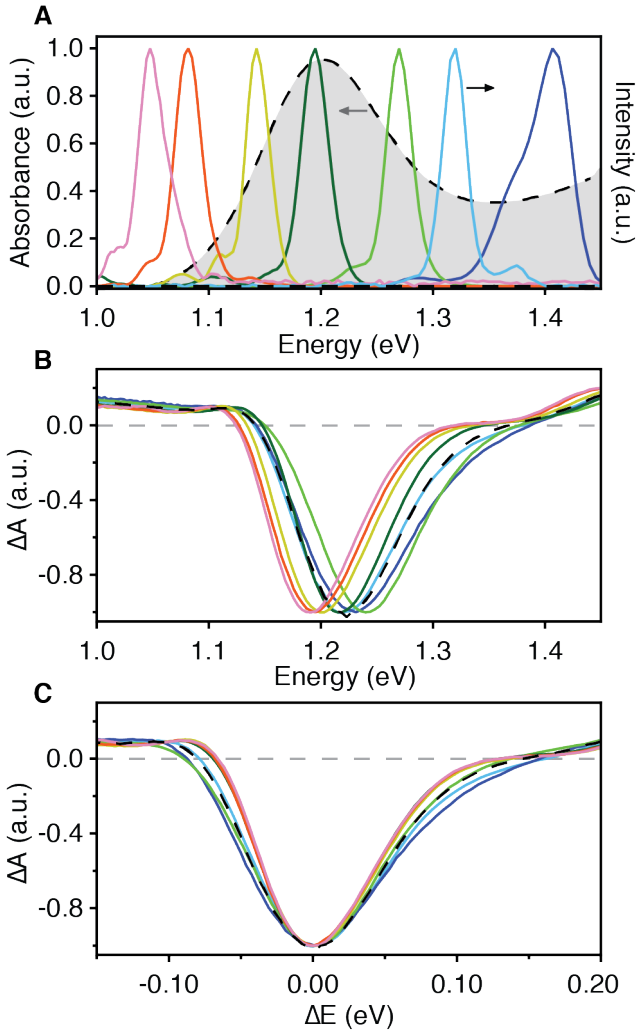

Figure 3. A) Nanocrystal extinction spectrum for an ensemble with E_g = 1.2 eV (dashed black line) and the spectra of the laser pulses used for photoexcitation. B) Transient spectra recorded at t = 2 ns as a function of photon energy. C) Transient spectra as a function of photon energy, offset to account for changes in the ground state bleach minima.

Given the narrow size distributions evident from the sharp spectral features in Figure 1B, we sought to estimate the single-particle spectral linewidth using transient spectral hole burning measurements.[43] Wavelength-tunable excitation pulses that are narrower than the $1S_e$–$1S_h$ linewidth of our samples (5–40 meV versus 65–320 meV) were used to selectively excite a fraction of the ensemble. Following pump-probe delay times (t = 2 ns) that are much longer than multiexciton lifetimes, we measure induced changes in the absorption spectrum (ΔA) as a function of the pump wavelength. Typical transient absorption (TA) spectra for an ensemble with E_g = 1.2 eV are plotted in Figure 3. As the excitation pulse is tuned from the tail of the $1S_e$–$1S_h$ absorption, where only the largest nanocrystals absorb, to higher energies, we observe a corresponding shift in the minimum of the ground state bleach signal (Figure 3B). After accounting for this shift (Figure 3C) and the finite spectral width of the excitation pulses (see Methods),[43] we deconvolute the transient absorption spectrum to determine the average single particle transient absorption linewidth. In all cases, this width is 17–27% narrower than that of the ensemble excited far above the band edge. We therefore estimate that the average single particle linewidth of the $1S_e$–$1S_h$ transition in the steady state absorption spectrum is 73–83% of the ensemble linewidth and conclude that the broadening due to the size distribution accounts for the remaining 17–27%.

Using the percent narrowing measured with TA, we calculate the intrinsic absorption linewidths of single sizes and plot them next to the ensemble linewidths in Figure 4A (see also: Figure S13). A recent measurement of the intrinsic average single particle linewidth ($1S_e$-$1S_h$ = 1.1 eV, FWHM = 141 meV) of a single size are in good agreement with our measurements.[44] A significant decrease in the broadening is evident as the size of the nanocrystal increases. The broadening derives from two affects: fine structure in the electronic states that contribute to the $1S_e$-$1S_h$ band and exciton phonon-coupling. Tight binding calculations on a series of particle sizes indicate that broadening caused by fine structure is size dependent may account for roughly half the observed broadening in Figure 4.[45] The remainder can be attributed to thermal broadening such as exciton phonon coupling, which is predicted to be stronger in small nanocrystals, although some disagreement exists over the magnitude of its size dependence.[46-50] Regardless of the source of the intrinsic spectral broadening, the data clearly show that the broadening caused by the size distribution is minor across the wide range of sizes accessible with the selenourea library.

Mechanistic studies of nanocrystal growth often use the spectral linewidth to argue for or against a particular growth mechanism: e.g. spectral broadening with increasing size is signature of Ostwald ripening, while spectral narrowing is signature of size distribution focusing. However, the size dependence of the single particle linewidth evident in Figure 4 and in other studies[51,52] must be considered in order to correctly extract the size distribution. In particular, the numerous claims of size distribution focusing should be reevaluated in light of our finding as well as related work on CdSe and PbS nanocrystals.[37] In the present case, the spectral linewidth is mostly a consequence of the intrinsic broadening of a single size and is not significantly influenced by the size distribution. Indeed, our estimate indicates that the relative standard deviation in the nanocrystal diameter is 0.5–2% for all samples studied here, corresponding to total distributions in the formula of 3–15 PbSe units, assuming a spherical particle shape. These distributions are vanishingly small and unlikely to induce significant differences in the relative growth rates within the size distribution.[52]

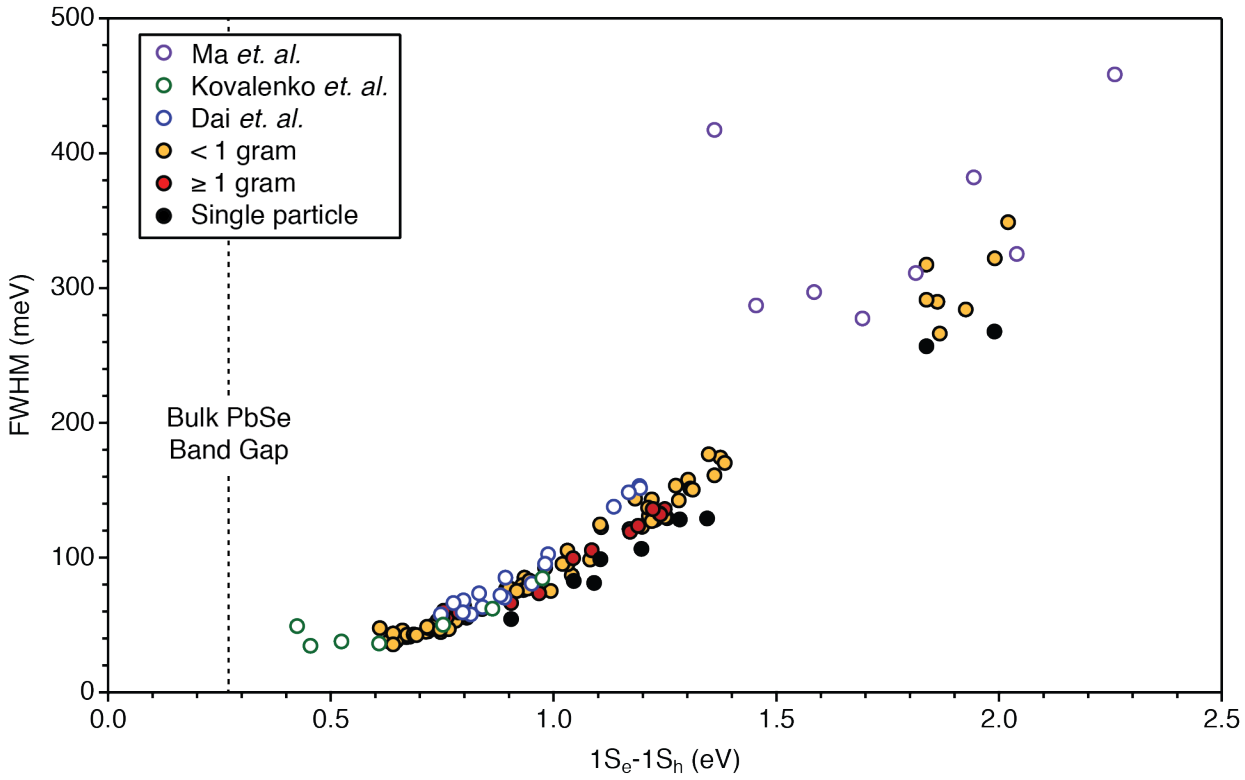

Figure 4. Results of a reproducibility study showing the FWHM of the lowest energy electronic transition versus its position ($1S_e$–$1S_h$) across 94 reactions using a variety of selenourea precursors and reaction scales (yellow, red). These data are overlaid with data extracted from previously published spectra of PbSe samples (violet,[30] green,[28] blue[29]) and single-particle component linewidths measured by spectral hole burning experiments (black).

CONCLUSIONS

We report a library of N,N,N'-trisubstituted selenoureas whose conversion kinetics to PbSe nanocrystals can be finely controlled by adjusting their substitution pattern. The nanocrystal concentration, and therefore the final nanocrystal size following complete precursor conversion, is readily tuned by the conversion reactivity. These precursors provide a convenient synthesis of PbSe nanocrystals on large reaction scales whose spectral features are exceptionally narrow and dominated by single-particle spectral broadening rather than the size distribution. This is especially valuable at small sizes where it has proven difficult to access PbSe nanocrystals whose band gap is appropriate for solar photovoltaic devices.

EXPERIMENTAL SECTION

General Methods. All manipulations were performed using standard air-free techniques on a Schlenk line under argon atmosphere or in a nitrogen-filled glovebox unless otherwise indicated.

Chemicals. Acetonitrile (≥99.5%), hexane (mixture of isomers, ≥98.5%), isopropanol (≥99.5%), methanol (≥99.8%), and toluene (≥99.5%) were obtained from Aldrich and used without further purification. Tetrachloroethylene (anhydrous, ≥99%), tetrahydrofuran (anhydrous, ≥99.9%, inhibitor-free), methyl acetate (99.5%, anhydrous), decane (anhydrous, ≥99%), dibutyl ether (anhydrous, 99.3%), diethylene glycol dimethyl ether ("diglyme," anhydrous, 99.5%) were obtained from Aldrich, transferred to a glovebox, shaken with activated alumina, filtered, and stored over activated 3Å molecular sieves for 24 h prior to use. Toluene (≥99.5), dichloromethane (≥99.5%, contains 40-150 ppm amylene as stabilizer), and diethyl ether (≥99.9%, inhibitor-free) were obtained from Aldrich, degassed, dried in a column packed with activated alumina, and stored in a glovebox over activated 3Å molecular sieves for 24 h prior to use. Pentane (≥98%) was obtained from Fisher Chemical, degassed, dried in a column packed with activated alumina, and stored in a glovebox over activated 3Å molecular sieves for 24 h prior to use. Diphenyl ether (≥99%), hexadecane (99%), and *n*-octane (≥99%) were obtained from Aldrich, stirred with calcium hydride overnight, distilled and stored in a glove box over activated 3Å molecular sieves for 24 h prior to use. 1-octene (99%) was obtained from Acros Organics, stirred with calcium hydride overnight, distilled and stored in a glove box over activated 3Å molecular sieves for 24 h prior to use. Benzene-d_6 (*d*, 99.5%), chloroform-*d* (*d*, 99.8%), dichloromethane-d_2 (*d*, 99.8%), tetrahydrofuran-d_8 (*d*, 99.5%), and toluene-d_8 (*d*, 99.5%) were obtained from Cambridge Isotope Laboratories and stored in a glovebox over activated 3Å molecular sieves for 24 h prior to use.

Diisopropylamine (≥99.5%), dibutylamine (≥99.5%), diethylamine (≥99.5%), pyrrolidine (≥99.5%, purified by distillation), piperidine (≥99.5%, purified by distillation), *N*-*n*-butylmethylamine (96%), diallylamine (99%), dimethylamine (2.0 M in tetrahydrofuran), Dicyclohexylamine (99%), *N*-ethylisopropylamine (98%), *N*-isopropylmethylamine (98%), *N*-ethylmethylamine (97%), 1,2,3,4-tetrahydroisoquinoline (95%), 4-chloro-*N*-methylaniline (97%), and *N*-methylaniline (98%) were obtained from Aldrich, stirred with calcium hydride overnight, distilled and stored in a glove box. 2-methylpyrrolidine (98%) was obtained from Acros Organics, stirred with calcium hydride overnight, distilled and stored in a glove box. 4-methoxy-*N*-methylaniline (98%) was obtained from Combi-Blocks, stirred with calcium hydride overnight, distilled and stored in a glove box. Dimethyl terephthalate (≥99%),

tris(dimethylamino)methane (97%), 4-(methylamino)benzonitrile (97%), and triethylamine (≥99%) were obtained from Aldrich and used without further purification. Selenium (100 mesh, 99.99%) and phosphorus(V) oxychloride (99%) were obtained from Aldrich and used without further purification. Lead(II) oxide (99.999+%) was obtained from Strem or Alfa Aesar and used without further purification. Cyclohexyl isocyanide (99%), *n*-butyl isocyanide (98+%), and *tert*-butyl isocyanide (97%) were obtained from Acros Organics, degassed by the freeze-pump-thaw method, and stored in a glovebox. Trifluoroacetic acid (99%) and trifluoroacetic anhydride (99%) were obtained from Aldrich and used without further purification. *N*-*n*-hexadecylformamide (97%) was obtained from Alfa Aesar and used without further purification. Oleic acid (99%) was obtained from Aldrich or Alfa Aesar, stored in a –20 °C freezer, and used without further purification.

Instrumentation. UV-Vis-NIR spectra were obtained using a Perkin-Elmer Lambda 950 spectrophotometer equipped with deuterium and halogen lamps and either a PbS or InGaAs detector. Samples for UV-Vis-NIR and photoluminescence spectroscopies were dissolved in tetrachloroethylene. A background spectrum was obtained of the same solvent mixture and concentration as the sample to be analyzed. Infrared photoluminescence measurements were conducted using excitation from a 6-picosecond supercontinuum laser. After spectral filtering, the excitation light (590 ± 10 nm, < 25 nJ cm^{-2} per pulse) was focused onto a dilute solution of nanocrystals. The emission was collected using reflective optics, dispersed by a 1/3-meter spectrometer, and detected with an InGaAs photodiode and lock-in amplifier. The grating angle was scanned to acquire spectra. All spectra were corrected for grating and detector efficiency, and the measurements were conducted under inert atmosphere with weak excitation and stirring to prevent experimental artifacts due to oxidation, multiple excitation, and photo-charging.

NMR spectroscopy was performed on Bruker 300, 400, and 500 MHz spectrometers. ^{77}Se NMR spectra were referenced to diphenyl diselenide in benzene-d_6 (464.10 ppm[53]), which was sealed inside a glass capillary and placed inside the NMR tube. Single crystal XRD analysis was performed on either an Agilent SuperNova SCXRD or a Bruker Apex II diffractometer. Powder XRD analysis was performed on a Scintag X-ray diffractometer. Transmission electron microscopy (TEM) was performed on either a JEOL JEM-100CX or a JEOL 2100 TEM.

Kinetics experiments were carried out under nitrogen at 9 mM in selenourea according to Hendricks *et al.*[13] Kinetics experiments were monitored at 400 nm using a PerkinElmer 316SS dip probe (2 mm path length) attached to a Perkin-Elmer Lambda 650 spectrophotometer equipped with deuterium and halogen lamps.

Transient spectral hole burning experiments were performed using a commercial amplified Ti:sapphire laser system (SpectraPhysics) operating at a repetition rate of 1 kHz. Resonant excitation pulses were generated by a collinear optical parametric amplifier (LightConversion) and the spectrum of each pulse was measured using a fiber coupled commercial miniature spectrometer (Ocean Optics NIRQuest). Near-infrared supercontinuum probe light was generated using a sapphire plate. Cross-polarized pump and probe beams were used to reject the scattered pump light. Transient spectra were recorded on a shot-by-shot basis using a pair of fiber coupled InGaAs (infrared) diode arrays (Ultrafast Systems). The excitation fluence in each measurement was approximately 100 μJ/cm^2.

Precursor synthesis. Lead oleate was prepared from lead trifluoroacetate according to Hendricks *et al.*[13] on 134 mmol scale. It is important to use high-purity, yellow lead(II) oxide in this reaction. *n*-Hexadecyl isocyanide was prepared according to Hoertz *et al.*[54] at 40 mmol scale. N,N,N'-N'-tetramethylselenourea was prepared according to Kantlehner, Hauber, and Vettel.[55]

Synthesis of selenoureas 1-31. In a glovebox, selenium (3.0 mmol), amine (3.0 mmol), isocyanide (3.0 mmol), and toluene (to a total volume of 3 mL) are sealed under nitrogen and the mixture stirred in an oil bath heated to 100 °C for 1 h. During this time nearly all of the selenium is consumed and the reaction mixture becomes colorless to yellow. The vessel is then transferred to a glovebox and, mixture is passed through a syringe filter (PTFE, 0.2 μm), and the volatiles are removed under vacuum. Solid selenoureas are recrystallized using solvents indicated in the Supplementary Information, isolated by filtration using a glass fritted funnel, and dried under vacuum for >3 h. Liquid and low-melting solid selenoureas area placed under vacuum for 24 h with stirring. Isolated selenoureas are stored at –40 °C in a glove box freezer where they are indefinitely stable. All reactions were performed at a 3.0 mmol scale unless otherwise noted, but can be run at 25 times the scale and twice the above concentrations without significantly impacting the results.

Example selenourea synthesis: N,N-dibutyl-N'-cyclohexylselenourea (16). N,N-dibutyl-N'-cyclohexylselenourea is prepared according to the general procedure from dibutylamine (387.7 mg, 3.00 mmol), selenium (236.9 mg, 3.00 mmol), and cyclohexyl isocyanide (327.5 mg, 3.00 mmol) in toluene (2.6 mL). The filtrate is recrystallized by concentration of a saturated solution in toluene under reduced pressure. The solid is isolated by suction filtration on a fritted glass funnel, washed with pentane (3 x 4 mL), and dried under vacuum for >3 h. White solid. Yield: 727.2 mg (76.4%).

Example selenourea synthesis: N'-cyclohexyl-N-ethyl-N-methylselenourea (18). N'-cyclohexyl-N-ethyl-N-methylselenourea was prepared according to the general procedure from N-ethylmethylamine (177.3 mg, 3.00 mmol), selenium (236.9 mg, 3.00 mL), and cyclohexyl isocyanide (327.5 mg, 3.00 mmol) in toluene (2.6 mL). Pentane (6 mL) is added to the filtrate to induce crystallization, and then the mixture is cooled in a –40 °C freezer for > 2 hours. Following this period, the crystals are isolated by suction filtration on a fritted glass funnel, washed with pentane (3 x 4 mL), and dried under vacuum >3 h. Pale yellow crystals. Yield: 0.5106 g (68.8%).

Example selenourea synthesis: N,N-diallyl-N'-butylselenourea (6). N,N-diallyl-N'-butylselenourea was prepared according to the general procedure from diallylamine (291.5 mg, 3.00 mmol), selenium (236.9 mg, 3.00 mmol), and butyl isocyanide (249.4 mg, 3.00 mmol) in toluene (2.6 mL). Pale yellow, nearly colorless oil. Yield: 757.2 mg (97.4%).

Synthesis of PbSe nanocrystals for absorbance and photoluminescence spectroscopies. In a glove box, lead oleate (231.0 mg, 0.30 mmol, 1.5 equiv) and 1-octene (9.5 mL) are added to a 40 mL scintillation vial equipped with a stir bar that is then sealed with a rubber septum. The selenourea (0.20 mmol) and diglyme (0.5 mL) are added to a 4 mL scintillation vial and sealed with a rubber septum. Both vials are removed from the glove box, the septa pierced with argon inlet needles, and placed in oil baths at 100 °C. After reaching thermal equilibrium (15 minutes), the selenourea

solution is injected into the lead oleate solution. An aliquot (100 μL) is removed at the desired time and dissolved in tetrachloroethylene (6 mL) for absorbance spectroscopy. For photoluminescence measurements, the reaction mixture is transferred via syringe into a Schlenk flask under argon, brought into a glove box, and diluted in tetrachloroethylene to an absorbance of 0.1–0.3 at the $1S_e$–$1S_h$ maximum.

Large-scale synthesis of 2.7 nm PbSe nanocrystals. In a glove box, lead oleate (2.657 g, 3.45 mmol, 1.5 equiv) and 1-octene (54.6 mL) are added to a 100 mL 3-neck round bottom flask equipped with a stir bar, that is then sealed with two rubber septa and an air-free vacuum adapter. In a 20 mL scintillation vial, N,N-dibutyl-N'-cyclohexylselenourea (0.730 g, 2.30 mmol) and dibutyl ether (2.9 mL) are mixed and the vial sealed with a rubber septum. Both vessels are transferred to a Schlenk line where they are placed under nitrogen and brought to 100 °C in an oil bath. Once the temperature is stable, the solution of selenourea is quickly injected into the clear colorless solution of lead oleate via a syringe equipped with a wide gauge needle. The reaction is allowed to run for 10 minutes before the flask is removed from the oil bath and allowed to cool to room temperature. The septa are then replaced with glass stoppers under positive argon flow and the volatiles removed under vacuum. After three hours, the flask is sealed and transferred to a nitrogen-filled glovebox. The dark residue is dissolved in 12 mL of a 1:1 pentane/toluene mixture. 50 mL of methyl acetate are added to precipitate the nanocrystals and the mixture is centrifuged (7000 rpm, 10 min), giving a clear, pale brown supernatant. The dark residue remaining is dissolved in 12 mL of a 1:1 pentane/toluene mixture, precipitated with 50 mL of methyl acetate, and centrifuged (7000 rpm, 10 min). This process is repeated three more times (five precipitations in total), and then the nanocrystal solution is dried under vacuum for > 6 hours. The nanocrystal solid is dissolved in benzene-d_6 or toluene-d_8 for analysis with UV-vis-NIR and NMR spectroscopies. Yield: 83-97%, based on empirical formulas of $(PbSe)(Pb(oleate)_2)_n$ determined spectroscopically. *Commercially available anhydrous octane (b.p. = 125-126°C) may also be used in place of 1-octene.*

Large-scale synthesis of 5.1 nm PbSe nanocrystals. In a glove box, lead oleate (10.497 g, 13.63 mmol, 1.2 equiv) and 1-octene (146 mL) are added to a 250 mL 3-neck round bottom flask equipped with a stir bar, that is then sealed with two rubber septa and an air-free vacuum adapter. To a 20 mL scintillation vial, N,N-diallyl-N'-butylselenourea (2.945 g, 11.36 mmol) and diglyme (5 mL), were added and the vial sealed with a rubber septum. Both vessels are transferred to a Schlenk line where they are placed under nitrogen and brought to 100 °C in an oil bath. Once the temperature is stable, the solution of selenourea is quickly injected into the clear colorless solution of lead oleate. The reaction is stirred for 120 minutes before the flask is removed from the oil bath and allowed to cool to room temperature. The septa are then replaced with glass stoppers under positive argon flow and the volatiles removed under vacuum. After two hours, the flask is placed under argon and the glass stoppers replaced with rubber septa. 50 mL of pentane is then added via cannula, and the dark slurry was transferred via cannula to a Teflon-sealable Schlenk flask and taken into a nitrogen glovebox. 70 mL of methyl acetate was added and the mixture was centrifuged (7000 rpm, 10 min.), giving a clear, pale brown supernatant. The dark residue remaining was dissolved in 65 mL of a 1:1 pentane/toluene mixture, precipitated with 135 mL of methyl acetate, and centrifuged (7000 rpm, 10 min.). The process of precipitation, centrifugation, and redissolution was repeated three more times. The nanocrystal solution was then dried under vacuum for 24 hours and the solid dissolved in a mixture of tetrachloroethylene and benzene-d_6 or toluene-d_8 for analysis with UV-vis-NIR and NMR spectroscopies. *Commercially available anhydrous octane (b.p. = 125-126°C) may also be used in place of 1-octene.*

Rate of Ostwald ripening experiment. Ostwald ripening was determined to be negligibly slow by following the same procedure described for the **synthesis of PbSe nanocrystals for absorbance and photoluminescence spectroscopies**. N,N-diallyl-N'-butylselenourea was injected into the lead oleate solution at 100 °C. Aliquots (200 μL) were removed at 2 hours, 5 hours, and 8 hours after injection and dissolved in tetrachloroethylene (6 mL) for absorbance spectroscopy.

Determination of oleate, PbSe, and nanocrystal concentrations. The concentrations of oleate, PbSe, and nanocrystals were determined by a combination of ^{1}H NMR and UV-Vis-NIR absorption spectroscopies. Purified nanocrystals are thoroughly dried under vacuum and dissolved in benzene-d_6 or toluene-d_8. Dimethyl terephthalate (DMT) dissolved in benzene-d_6 or toluene-d_8 (100 μL, 50.1 mM) was added to a known volume of the nanocrystal stock solution and its aromatic resonances used as an internal standard for ^{1}H NMR spectroscopy. The concentration of ligands was determined relative to the DMT internal standard by integrating the ligand vinyl and DMT aryl resonances and normalizing for the number of hydrogens, respectively (2:4). ^{1}H NMR spectra were acquired with sufficient relaxation delay to allow complete relaxation between pulses (T1(oleate vinyl) = 1.0 s; T1(DMT aryl) = 12.0 s; 5 x T1 = 60 s). See Figure S12 for an example ^{1}H NMR spectrum of isolated PbSe nanocrystals. The molar concentration of PbSe in these stock solutions was determined by diluting 10–50 μL to a known volume with tetrachloroethylene and measuring the absorbance at λ = 400 nm. At this wavelength, the extinction coefficient is independent of size.[8]

Determination of the number of ligands per nanocrystal and PbSe units per nanocrystal. The wavelength of the lowest energy absorption maximum was used to determine the average nanocrystal diameter.[29] Assuming the nanocrystals have a spherical shape and the molar volume of bulk PbSe, the number of PbSe units per nanocrystal was calculated from the nanocrystal diameter. The concentration of nanocrystals, the ratio of ligands per nanocrystal, and the ligand surface density were calculated from the number of PbSe units per nanocrystal, the molar concentration of PbSe, and ligands in the stock solution.

Estimation of single-particle linewidths. To estimate the linewidths of the nanocrystal electronic transitions, we use a modified version of the transient spectral hole burning experiments described in Norris *et al.*[43] Briefly, features in the t = 2 ns transient absorption spectra are fit using a negative amplitude Gaussian function bordered by two positive amplitude Gaussian functions. The positive functions account for spectral shifts associated with the excited state of the quantum dot (also known as the biexciton effect).[43,56,57] A linear baseline was used to account for the background photoinduced absorption signals. A typical spectral decomposition is shown in Figure S14. In all cases, the linewidth of the transition is taken to be the width of the negative Gaussian signal component (with variance $\sigma^2_{measured}$).

We account for the finite width of the laser pulse spectrum using by fitting it to a Gaussian lineshape (whose variance is σ^2_{laser}).

Deconvolution is used to obtain the corrected linewidths (with variance of $\sigma^2_{particle}$) as a function of excitation energy:

$$\sigma^2_{measured} = \sigma^2_{laser} + \sigma^2_{particle}$$

The finite bandwidth of the laser pulse minimally affects the measured linewidth. For the sample with E_g = 1.2 eV shown in the main text, the measured and deconvoluted linewidths differ by only 5%. This is a typical value for the range of samples reported here (2–7% difference). The high excitation energy ensemble linewidth is independent of the laser pulse spectrum since the spectrum is featureless and absorbs roughly equally over the excitation pulse width in that spectral region. As such, no deconvolution of the laser lineshape is used to determine the ensemble widths (extracted using the Gaussian fitting procedure described above).

The $1S_e$–$1S_h$ transition is fit to a Gaussian function on an eV scale. The resulting c (width) parameter is multiplied by the percent narrowing obtained from spectral hole burning measurements, giving the homogeneous linewidth c_0. The inhomogeneous broadening is expressed as $c - c_0$ (in eV) and plotted in Figure 4 in the main text.

Estimation of relative standard deviation (%RSD). The absorption spectrum is converted to nanocrystal diameter according to Dai *et al.*[29]:

$$d = (\lambda - 143.75)/281.25$$

where d is the nanocrystal diameter in nanometers. The $1S_e$–$1S_h$ transition within this plot is fit to a Gaussian function and from which c is multiplied by the percent narrowing obtained from spectral hole burning measurements, giving the single-particle linewidth c_0 (in nm). These parameters are used to obtain a relative (%) standard deviation in diameter:

$$\%RSD = \frac{c - c_0}{d}$$

where d is the average nanocrystal diameter. d is also converted to a number of PbSe formula units per nanocrystal at each point:

$$n_{PbSe} = \frac{V_{NC}Z}{V_{UC}} = \frac{\pi d^3 Z}{6V_{UC}}$$

Where n_{PbSe} is the average number of PbSe formula units per nanocrystal, V_{NC} is the average nanocrystal volume in nm^3 (assuming sphericity), Z is the number of PbSe formula units per unit cell ($Z = 4$ for rock salt PbSe), and V_{UC} is the volume of the PbSe unit cell (0.0584925 nm^3). The c parameter extracted from Gaussian fit on this axis is multiplied by 1 minus the percent narrowing obtained from spectral hole burning measurements, giving the homogeneous linewidth c_0 in terms of n_{PbSe}. The inhomogeneous broadening is again expressed as $c - c_0$, giving the standard deviation in n_{PbSe}. These values are plotted in Figures 4B and 4C in the main text.

ASSOCIATED CONTENT

Supporting Information

The Supporting Information is available free of charge on the ACS Publications website.

NMR spectra, UV-vis-NIR spectra, photoluminescence spectra, kinetics data, reproducibility plots, surface ligand coverage calculations, hole burning spectra and fits, precursor characterization, and crystallographic data (PDF)

AUTHOR INFORMATION

Corresponding Author

* E-mail: jso2115@columbia.edu

Author Contributions

M.P.C., R.A.S., and G.T.C. synthesized selenoureas. A.N.B. performed and analyzed the X-ray crystallographic measurements. M.P.C. designed, performed, and analyzed the nanocrystal synthesis experiments and surface chemistry measurements. M.P.C. and M.P.H. designed, performed, and analyzed the kinetics experiments. M.Y.S. designed, performed, and analyzed the transient absorption measurements. M.P.C. and J.S.O. co-wrote the paper with support from all co-authors.

Notes

The authors declare no competing financial interest.

ACKNOWLEDGMENTS

The precursor library development and reaction kinetics were supported by the National Science Foundation under grant CHE-1151172. Large scale synthesis and surface ligand analysis was supported by the Department of Energy under grant DE-SC0006410. Evelyn Auyeung performed transmission electron microscope measurements on a JEOL 2100 instrument. Ilan Jen-La Plante performed transmission electron microscope measurements on a JEOL 2100F instrument at the New York Structural Biology Center (NYSBC). NYSBC is supported by NYSTAR and the Research Facilities Improvement Program C06 RR017528-01-CEM from the National Center for Research Resources, National Institutes of Health. We thank J. Palmer and G. Parkin for assistance with X-ray crystallography and the National Science Foundation (CHE-0619638) for acquisition of an X-ray diffractometer. We thank Daniel W. Paley for helpful discussions regarding crystallography and Columbia University's Shared Materials Characterization Lab for the use of X-ray equipment essential to this research. We thank E. Busby for assistance with NIR photoluminescence. This research used resources of the Center for Functional Nanomaterials, which is a U.S. DOE Office of Science Facility, at Brookhaven National Laboratory under Contract No. DE-SC0012704.

REFERENCES

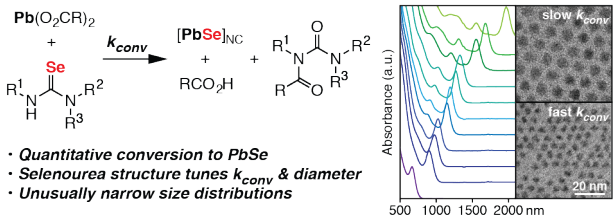

(1) Nozik, A. J. *Physica E: Low-dimensional Systems and Nanostructures* **2002**, *14*, 115.

(2) Carey, G. H.; Abdelhady, A. L.; Ning, Z.; Thon, S. M.; Bakr, O. M.; Sargent, E. H. *Chem. Rev.* **2015**, *115* (23), 12732.

(3) Semonin, O. E.; Luther, J. M.; Choi, S.; Chen, H. Y.; Gao, J.; Nozik, A. J.; Beard, M. C. *Science* **2011**, *334* (6062), 1530.

(4) Boneschanscher, M. P.; Evers, W. H.; Geuchies, J. J.; Altantzis, T.; Goris, B.; Rabouw, F. T.; van Rossum, S. A. P.; van der Zant, H. S. J.; Siebbeles, L. D. A.; Van Tendeloo, G.; Swart, I.; Hilhorst, J.; Petukhov, A. V.; Bals, S.; Vanmaekelbergh, D. *Science* **2014**, *344* (6190), 1377.

(5) Evers, W. H.; Schins, J. M.; Aerts, M.; Kulkarni, A.; Capiod, P.; Berthe, M.; Grandidier, B.; Delerue, C.; van der Zant, H. S. J.; van Overbeek, C.; Peters, J. L.; Vanmaekelbergh, D.; Siebbeles, L. D. A. *Nature Communications* **2015**, *6*, 1.

(6) Kalesaki, E.; Delerue, C.; Morais Smith, C.; Beugeling, W.; Allan, G.; Vanmaekelbergh, D. *Phys. Rev. X* **2014**, *4* (1), 011010.

(7) Delerue, C. *Nature Materials* **2016**, *15* (5), 498.

(8) Moreels, I.; Lambert, K.; De Muynck, D.; Vanhaecke, F.; Poelman, D.; Martins, J. C.; Allan, G.; Hens, Z. *Chemistry of Materials* **2007**, *19* (25), 6101.

(9) Steckel, J. S.; Yen, B. K. H.; Oertel, D. C.; Bawendi, M. G. *J. Am. Chem. Soc.* **2006**, *128* (40), 13032.

(10) Evans, C. M.; Evans, M. E.; Krauss, T. D. *J. Am. Chem. Soc.* **2010**, *132* (32), 10973.

(11) Zhang, J.; Gao, J.; Miller, E. M.; Luther, J. M.; Beard, M. C. *ACS Nano* **2014**, *8* (1), 614.

(12) Joo, J.; Pietryga, J. M.; McGuire, J. A.; Jeon, S.-H.; Williams, D. J.; Wang, H.-L.; Klimov, V. I. *J. Am. Chem. Soc.* **2009**, *131* (30), 10620.

(13) Hendricks, M. P.; Campos, M. P.; Cleveland, G. T.; Jen-La Plante, I.; Owen, J. S. *Science* **2015**, *348* (6240), 1226.

(14) Sugimoto, T. *Journal of Colloid And Interface Science* **1992**, *150*, 208.

(15) Sugimoto, T.; Shiba, F.; Sekiguchi, T.; Itoh, H. *Colloids and Surfaces A: Physicochemical and Engineering Aspects* **2000**, *164*, 183.

(16) Owen, J. S.; Chan, E. M.; Liu, H.; Alivisatos, A. P. *J. Am. Chem. Soc.* **2010**, *132* (51), 18206.

(17) Abe, S.; Capek, R. K.; De Geyter, B.; Hens, Z. *ACS Nano* **2012**, *6* (1), 42.

(18) Koketsu, M.; Ishihara, H. In *Handbook of Chalcogen Chemistry: New Perspectives in Sulfur, Selenium and Tellurium*; Devillanova, F. A., Ed.; Royal Society of Chemistry: Cambridge, 2007; pp 145–194.

(19) Lipp, M.; Dallacker, F.; Köcker, I. Z. *Monatshefte für Chemie und verwandte Teile anderer Wissenschaften* **1959**, *90* (1), 41.

(20) Sonoda, N.; Yamamoto, G.; Tsutsumi, S. *Bulletin of the Chemical Society of Japan*

1972, *45*, 2937.
(21) Blum, T.; Ermert, J.; Coenen, H. H. *Journal of Labelled Compounds and Radiopharmaceuticals* **2001**, *44* (Supplement S1), S140.
(22) Mamedov, V. A.; Zhukova, N. A.; Gubaidullin, A. T.; Beschastnova, T. N.; Rizvanov, I. K.; Levin, Y. A.; Litvinov, I. A. *Russian Chemical Bulletin* **2010**, *58* (6), 1294.
(23) Palmer, J. H.; Parkin, G. *Polyhedron* **2013**, *52* (C), 658.
(24) Zakrzewski, J.; Huras, B.; Kiełczewska, A. *Synthesis* **2015**, *48* (01), 85.
(25) Landry, V. K.; Minoura, M.; Pang, K.; Buccella, D.; Kelly, B. V.; Parkin, G. *J. Am. Chem. Soc.* **2006**, *128* (38), 12490.
(26) Murray, C. B.; Sun, S.; Gaschler, W.; Doyle, H.; Betley, T. A.; Kagan, C. R. *IBM Journal of Research and Development* **2001**, *45* (1), 47.
(27) Yu, W. W.; Falkner, J. C.; Shih, B. S.; Colvin, V. L. *Chemistry of Materials* **2004**, *16* (17), 3318.
(28) Kovalenko, M. V.; Talapin, D. V.; Loi, M. A.; Cordella, F.; Hesser, G.; Bodnarchuk, M. I.; Heiss, W. *Angew. Chem. Int. Ed.* **2008**, *47* (16), 3029.
(29) Dai, Q.; Wang, Y.; Li, X.; Zhang, Y.; Pellegrino, D. J.; Zhao, M.; Zou, B.; Seo, J.; Wang, Y.; Yu, W. W. *ACS Nano* **2009**, *3* (6), 1518.
(30) Ma, W.; Swisher, S. L.; Ewers, T.; Engel, J.; Ferry, V. E.; Atwater, H. A.; Alivisatos, A. P. *ACS Nano* **2011**, *5* (10), 8140.
(31) Choi, J. J.; Lim, Y.-F.; Santiago-Berrios, M. B.; Oh, M.; Hyun, B.-R.; Sun, L.; Bartnik, A. C.; Goedhart, A.; Malliaras, G. G.; Abruña, H. D.; Wise, F. W.; Hanrath, T. *Nano Lett.* **2009**, *9* (11), 3749.
(32) Evans, C. M.; Guo, L.; Peterson, J. J.; Maccagnano-Zacher, S.; Krauss, T. D. *Nano Lett.* **2008**, *8* (9), 2896.
(33) Hendricks, M. P.; Cossairt, B. M.; Owen, J. S. *ACS Nano* **2012**, *6* (11), 10054.
(34) Campos, M. P.; Owen, J. S. *Chemistry of Materials* **2016**, *28* (1), 227.
(35) Anderson, N. C.; Hendricks, M. P.; Choi, J. J.; Owen, J. S. *J. Am. Chem. Soc.* **2013**, *135* (49), 18536.
(36) Busby, E.; Anderson, N. C.; Owen, J. S.; Sfeir, M. Y. *J. Phys. Chem. C* **2015**, *119* (49), 27797.
(37) Peng, X.; Wickham, J.; Alivisatos, A. P. *J. Am. Chem. Soc.* **1998**, *120*, 5343.
(38) Weidman, M. C.; Beck, M. E.; Hoffman, R. S.; Prins, F.; Tisdale, W. A. *ACS Nano* **2014**, *8* (6), 6363.
(39) Cui, J.; Beyler, A. P.; Marshall, L. F.; Chen, O.; Harris, D. K.; Wanger, D. D.; Brokmann, X.; Bawendi, M. G. *Nature Chemistry* **2013**, *5* (7), 602.
(40) Cui, J.; Beyler, A. P.; Coropceanu, I.; Cleary, L.; Avila, T. R.; Chen, Y.; Cordero, J. M.; Heathcote, S. L.; Harris, D. K.; Chen, O.; Cao, J.; Bawendi, M. G. *Nano Lett.* **2016**, *16* (1), 289.
(41) Chen, O.; Zhao, J.; Chauhan, V. P.; Cui, J.; Wong, C.; Harris, D. K.; Wei, H.; Han, H.-S.; Fukumura, D.; Jain, R. K.; Bawendi, M. G. *Nature Materials* **2013**, *12* (1), 445.
(42) Beecher, A. N.; Yang, X.; Palmer, J. H.; LaGrassa, A. L.; Juhas, P.; Billinge, S. J. L.; Owen, J. S. *J. Am. Chem. Soc.* **2014**, *136* (30), 10645.
(43) Norris, D. J.; Sacra, A.; Murray, C. B.; Bawendi, M. G. *Phys. Rev. Lett.* **1994**, *72* (16), 2612.
(44) Park, S. D.; Baranov, D.; Halder, A.; Seifert, S.; Vajda, S.; Jonas, D. M. *Unpublished*.
(45) Allan, G.; Delerue, C. *Phys. Rev. B* **2004**, *70* (24), 245321.
(46) Kelley, A. M. *J. Phys. Chem. Lett.* **2010**, *1* (9), 1296.
(47) Kelley, A. M. *ACS Nano* **2011**, *5* (6), 5254.
(48) Lin, C.; Gong, K.; Kelley, D. F.; Kelley, A. M. *J. Phys. Chem. C* **2015**, *119* (13), 7491.

(49) Salvador, M. R.; Graham, M. W.; Scholes, G. D. *J. Chem. Phys.* **2006**, *125* (18), 184709.
(50) Sagar, D. M.; Cooney, R. R.; Sewall, S. L.; Dias, E. A.; Barsan, M. M.; Butler, I. S.; Kambhampati, P. *Phys. Rev. B* **2008**, *77* (23), 235321.
(51) Bullen, C. R.; Mulvaney, P. *Nano Lett.* **2004**, *4* (12), 2303.
(52) Clark, M. D.; Kumar, S. K.; Owen, J. S.; Chan, E. M. *Nano Lett.* **2011**, *11* (5), 1976.
(53) Badiello, R.; Batt, L.; Bergman, J.; Chakraborti, D.; Gsizmadia, I. G.; Engman, L.; Fringuelli, F.; Fujimori, K.; Gross, M. L.; Gysling, H. J.; Hargittai, I.; Hevesi, L.; Irgolic, K. J.; Jensen, K. A.; Kjaer, A.; Luthra, N. P.; Oae, S.; Odom, J. D.; Ogawa, A.; Okamoto, Y.; Poirier, R. A.; Renson, M.; Rozsondai, B.; Sidén, J.; Snatzke, G.; Sonoda, N.; Sturgeon, G. D.; Taticchi, A.; A, Z. R. *The Chemistry of Organic Selenium and Tellurium Compounds*; Padai, S., Rappoport, Z., Eds.; John Wiley & Sons: Chichester, Great Britain, 1986; Vol. 1.
(54) Hoertz, P. G.; Niskala, J. R.; Dai, P.; Black, H. T.; You, W. *J. Am. Chem. Soc.* **2008**, *130* (30), 9763.
(55) Kantlehner, W.; Hauber, M.; Vettel, M. *Journal fur praktische Chemie Chemiker-Zeitung* **1996**, 403.
(56) Hu, Y.; Koch, S.; Lindberg, M.; Peyghambarian, N.; Pollock, E.; Abraham, F. *Phys. Rev. Lett.* **1990**, *64* (15), 1805.
(57) Klimov, V.; Hunsche, S.; Kurz, H. *Phys. Rev. B* **1994**.